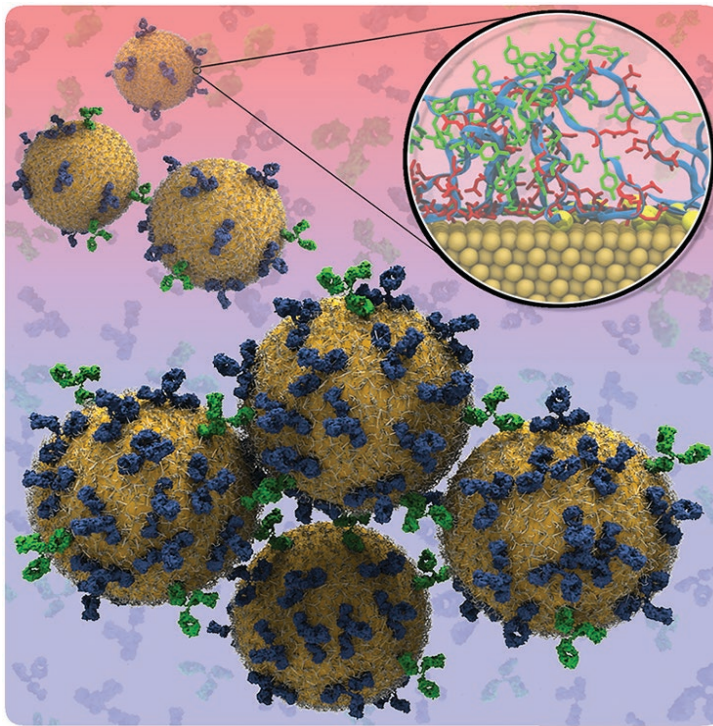


# Understanding and Designing the Gold–Bio Interface: Insights from Simulations

Patrick Charchar, Andrew J. Christofferson, Nevena Todorova, and Irene Yarovsky\*



## From the Contents

1. Introduction .....	2
2. Electronic Structure Calculations.....	2
3. All-Atom Molecular Mechanics and Dynamics (Force Field Methods) .....	8
4. Coarse-Grained and Simplified Approaches .....	12
5. Enhanced Sampling Techniques.....	13
6. Applications .....	13
7. Conclusions and Perspectives.....	19

**G**old nanoparticles (AuNPs) are an integral part of many exciting and novel biomedical applications, sparking the urgent need for a thorough understanding of the physicochemical interactions occurring between these inorganic materials, their functional layers, and the biological species they interact with. Computational approaches are instrumental in providing the necessary molecular insight into the structural and dynamic behavior of the Au–bio interface with spatial and temporal resolutions not yet achievable in the laboratory, and are able to facilitate a rational approach to AuNP design for specific applications. A perspective of the current successes and challenges associated with the multiscale computational treatment of Au–bio interfacial systems, from electronic structure calculations to force field methods, is provided to illustrate the links between different approaches and their relationship to experiment and applications.

## 1. Introduction

Gold nanomaterials show enormous potential to provide significant biomedical advancements in biosensing,<sup>[1]</sup> bio-imaging,<sup>[2]</sup> drug-delivery,<sup>[3]</sup> magnetic and photothermal therapies,<sup>[4]</sup> antimicrobial devices<sup>[5]</sup> as well as many other novel medical diagnostic and treatment technologies.<sup>[6]</sup> The widespread applicability of gold nanoparticles (AuNPs) and nanoclusters (AuNCs) within these diverse contexts is largely owing to the unique size-dependent chemical, physical and optical properties they exhibit, along with the ease in which they can be functionalized by biologically relevant chemistries.<sup>[7]</sup> In order to rationally design and optimize AuNPs for incorporation and efficiency within biomedical devices and *in vivo*, there is a need to thoroughly understand how these materials and their properties adjust in biological media (plasma, cell membranes and, ideally, various intracellular environments) as well as how the components of biological milieu (water, proteins, lipid bilayers, DNA) respond to the presence of AuNPs. Therefore, the fundamental physicochemical description of the gold–bio interface should in principle involve multiple time and length scale regimes commensurate with the physicochemical phenomena occurring at this interface (**Figure 1**). These range from charge transfer reactions<sup>[8]</sup> that take place at femtosecond time scales and angstrom resolutions to ligand exchanges,<sup>[9]</sup> AuNP reconstructions<sup>[10]</sup> and biomolecular conformational changes<sup>[11]</sup> that can transpire over milliseconds to hours and span across tens of nanometers. An excellent description of the relevance each time and length scale has to the physics and chemistry of nano–bio interfaces is provided in reference.<sup>[12]</sup> Despite significant recent advancements in experimental characterization techniques,<sup>[13]</sup> a comprehensive multiscale understanding of the structure and dynamics at the Au–bio interface relevant to biomolecular and physiological responses is still lacking.

State of the art engineering of efficient and safe Au nanomaterials for both *in vitro* and *in vivo* applications has recently been described from the experimental perspective<sup>[1a,7,17]</sup> and involves multiple levels of design challenges. These include the careful selection of the metallic Au core size and functional layer (peptides, antibodies, DNA, organic and other ligands); the solvent/buffer composition; application of external forces such as mechanical stresses, electric and magnetic fields; and even the choice of the biological environment itself (plasma/lipid membranes). The latter is expected to influence “hard” and “soft” corona formation on the NP surface as the particles progress through *in vivo* pathways or experience biological fluids during *in vitro* applications.<sup>[17c,18]</sup> Therefore the design and optimization of AuNP-biomaterials requires the fine-tuning of the physical forces responsible for both specific and non-specific gold–bio molecular interactions (**Table 1**). The aim is to maximize specific interactions essential for selective targeting and molecular recognition while discouraging non-specific interactions in order to avoid unwanted corona formation *in vivo* and potential adverse effects due to the loss of control over NP functionality and selectivity. It is thus essential to understand the effect atomistic make-up has on the structural and dynamic behavior of the AuNP–bio interface, which necessitates the employment

of theoretical and computational approaches to complement experiments at multiple time scales, length scales and levels of detail not yet achievable in the laboratory (Figure 1).

Indeed, while the number of computational works targeting the Au–bio interface at varying levels of theory has drastically increased in recent years, an all-encompassing comprehensive knowledge of these systems has not yet been realized. This is largely due to serious challenges associated with the computational approaches themselves as well as the huge variability in possible Au nanomaterials and even greater variety in their biomedical applications. The purpose of this review is to describe the current advances and challenges associated with the theoretical computational treatment of Au–bio interfacial systems and to illustrate the applicability and links between different approaches employed to investigate AuNP and AuNP–bio systems. This will help put the current state of the field into perspective for interested experimentalists, as well as computational practitioners, to encourage and enable cross-disciplinary collaborations.

## 2. Electronic Structure Calculations

Of the computational approaches available, those based on quantum mechanics (QM) provide the most accurate and precise information about molecular systems via their explicit consideration of the electronic structure, and include the wavefunction<sup>[19]</sup> and density functional theory<sup>[20]</sup> (DFT) formalisms, which have been described comprehensively in the literature.<sup>[21]</sup> In the context of Au nanomaterials, QM calculations are primarily used for AuNP structure determination, analysis of electronic and optical properties, chemical functionalization and force field (FF) parameterization for molecular mechanics (MM) and molecular dynamics (MD) simulations. Although several recent reviews discuss the role of QM calculations in describing structural, morphological and optical properties of Au surfaces and particles,<sup>[22]</sup> we would like to emphasize key points of general interest to computational practitioners, as well as considerations specific to modeling nano Au–bio interactions.

### 2.1. Structure Determination

Structure determination is of great importance as knowledge of the exact atomic arrangement is critical for understanding the physical and chemical properties of molecules and materials.<sup>[23]</sup> One of the most significant early successes was the full structure determination of the Au<sub>25</sub> nanocluster using

P. Charchar, Dr. A. J. Christofferson, Dr. N. Todorova,  
Prof. I. Yarovsky  
School of Engineering  
RMIT University  
Melbourne, Victoria 3001, Australia  
E-mail: irene.yarovsky@rmit.edu.au



DOI: 10.1002/smll.201503585

DFT (**Figure 2**),<sup>[24]</sup> which was subsequently confirmed by X-ray crystallography.<sup>[16b,25]</sup> In their theoretical work, Akola et al. calculated electron affinities and ionization potentials of three DFT optimized  $\text{Au}_{25}(\text{SR})_{18}$  isomers as guidelines to ascertain the lowest energy structure, as well as compared their calculated X-ray diffraction (XRD) patterns and optical gaps to experimental XRD data. This study highlights the value in not only comparing calculated results to available experimental data when undergoing theoretical structure determination, but also in using experimental data to provide guidelines in the geometry optimization process. Similarly, in 2010 the structure of  $\text{Au}_{38}(\text{SR})_{24}$  was successfully determined using DFT<sup>[26]</sup> just prior to the resolution of the X-ray crystal structure.<sup>[27]</sup> The revolutionary finding in these early studies was that the thiolated AuNC assemblies exhibited highly symmetric gold cores that are surrounded by adatom gold “staples” (Figure 2). This view of AuNC morphology was quite contrasting to previous models that proposed thiolates simply formed a protective layer on the cluster surfaces.<sup>[22c]</sup> More recently, this “staple” motif has been shown to consistently appear in many other structures determined through a combination of experimental and computational methods, including:  $\text{Au}_{22}(\text{SR})_{18}$ ,<sup>[28]</sup>  $\text{Au}_{67}(\text{SR})_{35}$ ,<sup>[29]</sup>  $\text{Au}_{144}(\text{SR})_{60}$ ,<sup>[30]</sup>  $\text{Au}_{147}(\text{SR})_n$  ( $n = 0, 12, 24, 50, 72$ ),<sup>[31]</sup>  $\text{Au}_{187}(\text{SR})_{68}$ ,<sup>[32]</sup> and  $\text{Au}_{333}(\text{SR})_{79}$ ,<sup>[33]</sup> as well as on planar Au surfaces.<sup>[34]</sup>

In the context of stability, the superatom complex model can be very useful in predicting the empirical composition of stable AuNCs.<sup>[35]</sup> Briefly, a given cluster  $[\text{Au}_m(\text{SR})_n]^q$  is found to exhibit exceptional stability if the number of free gold valence electrons  $N$  is a “magic number” corresponding to a closed-shell electron count (2, 8, 18, 20, 34, 58, etc.). This can be calculated based on  $N = m - n - q$ , where  $m$  is the number of Au(6s<sup>1</sup>) electrons,  $n$  is the number of thiol motifs and  $q$  is the net charge of the cluster. While AuNCs such as  $[\text{Au}_{25}(\text{SR})_{18}]^{-1}$  and  $[\text{Au}_{102}(\text{SR})_{44}]^0$  correspond to magic numbers (8 and 58 respectively), others such as  $[\text{Au}_{25}(\text{SR})_{18}]^0$  and  $[\text{Au}_{38}(\text{SR})_{24}]^0$  do not, even though they are still found to be stable experimentally. Negishi et al. offered an explanation that nanocluster stability is due to geometric rather than electronic factors.<sup>[36]</sup> In other words, magic numbers may serve as a guideline in proposing stable structures such as  $[\text{Au}_{25}(\text{SR})_{18}]^{-1}$ , but it is ultimately the icosahedral geometry of the  $\text{Au}_{25}$  core, rather than the electronic configuration alone, that is responsible for the stability. Further discussion on magic numbers and “staple fitness” as a method of structure prediction may be found in a review by De-en Jiang.<sup>[22d]</sup>

In general, AuNCs are typically defined as AuNPs with a core diameter of less than 3 nm and characteristically feature discrete electronic-level structuring and molecule-like properties.<sup>[22a]</sup> This is illustrated by the recent combined experimental and computational work of Negishi et al. wherein the transition point from bulk-like structures with plasmonic absorption behavior to molecule-like structures with quantized electronic behavior (**Figure 3**) of dodecanethiolate-protected AuNCs was found to occur between 187 and 144 gold atoms.<sup>[37]</sup> However, it has been shown that a plasmon-like response may be produced by AuNCs with as few as 23 Au atoms by changing the nature of the ligand.<sup>[38]</sup> Further investigation is therefore required to establish the



**Irene Yarovsky** is currently Professor of Theoretical Physics at RMIT University, Melbourne, Australia. She completed her PhD in Monash University in 1995 and then joined BHP Research Laboratory where she applied computational modeling to help design advanced industrial materials. Following her industry appointment, Irene joined RMIT University where from 2000 she has been leading a research group in theory and simulation of materials with a strong application focus, ranging from industrial to bio-materials and novel nanomaterials. At present, she is particularly

interested in studying the interface between biological systems and nanomaterials as they interact in living organisms, the environment and novel nano-bio devices for biomedical applications.

**Patrick Charchar** is a PhD student, **Nevena Todorova** and **Andrew Christofferson** are Research Fellows in the Yarovsky group at RMIT University.

characteristics of this transition for different thiol and other functionalized ligands (e.g., selenoate groups<sup>[39]</sup>), and it is through structural studies like these that our knowledge regarding the origin of the intrinsic size-dependent properties of gold grows.

When using the DFT approach, it should be noted that the choice of functional employed is extremely important. Muniz-Miranda et al. assessed the ability of different exchange-correlation functionals to reproduce the X-ray crystal data of organic-protected AuNCs in an extensive benchmarking study<sup>[40]</sup> and found that GGA functionals with PBE-like electron correlation treatment, used with the modified LANL2DZ pseudopotential and basis set,<sup>[41]</sup> produced good agreement with experiment for several nanoclusters. They also commented that functionals with the LYP correlation (e.g., BLYP, B3LYP) tended to deform cluster geometry during optimization. Regardless of the method used, it is critical to take relativistic effects into account in order to obtain accurate structural and electronic properties of Au nanomaterials. For an in-depth discussion of relativistic effects please see references.<sup>[22c,42]</sup> In addition to effective core potentials such as the aforementioned LANL2DZ, meaningful quasi-relativistic calculations can also be achieved using all-electron methods such as ZORA and DKH.<sup>[43]</sup>

It is important to be aware that the lowest-energy structure found by DFT geometry optimization is not necessarily the one found in nature. For example, in 2012 Pei et al. proposed an interlocked catenane-like arrangement for  $\text{Au}_{24}(\text{SR})_{20}$  based on their DFT studies,<sup>[44]</sup> but in 2014 Das et al. determined the X-ray crystal structure<sup>[45]</sup> and found that it did not match the predicted lowest-energy model. Interestingly, it did match the calculated third-lowest energy structure (labeled Iso3 in Pei et al.). Despite the potential limitations, DFT remains an invaluable tool for structure determination, particularly since not all AuNPs diffract to atomic resolution. This is highlighted in the work of Azubel et al. where  $\text{Au}_{68}$  NPs were unresolved below 5 Å using XRD. Instead, linear-response, time-dependent DFT (LR-TDDFT) provided a means to verify the proposed theoretical structure through

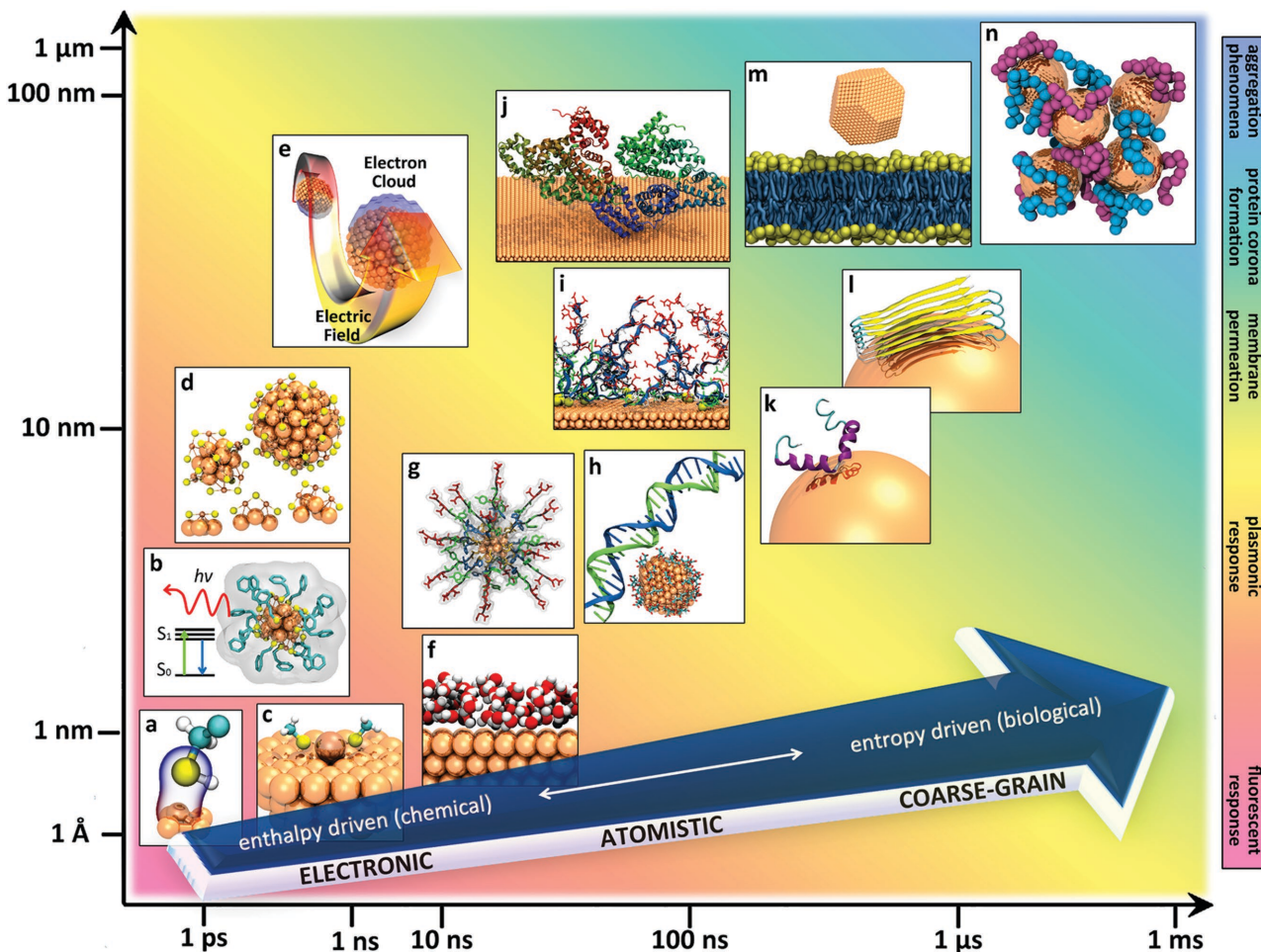


**Figure 1.** Schematic illustrating molecular models (a–n) and simulation approaches (blue arrow) aiming to capture physicochemical interactions at the interface between gold nanomaterials and biological matter at chemically and biologically relevant time and length scales: a) Au surface functionalization reactions, b) AuNC electronic excitation and fluorescence, c) AuNP growth and surface reconstruction, d) AuNP structure/morphology, e) AuNP surface plasmon resonance, f) Au-solvent interactions and polarization, g–l) biomolecular interactions and adsorption on Au surfaces and NP, including (in order of appearance) grafted functional chains/peptides, DNA, self-assembled monolayers, protein complexes, individual proteins, fibrillar protein aggregates, m) AuNP-lipid membrane interactions and internalization mechanisms, and n) AuNP aggregation. The relevance of the models and simulation methods to biomedical applications of gold is indicated by the spectrum of background color. The temporal and spatial resolution shown on the axes reflect the scale of the AuNP properties (a–n) and the blue arrow is (currently) indicative of the modeling approaches capable to treat the respective phenomena, however the latter can be expected to change (i.e., each method will move up the time and length scales) with further increase of high-performance computing capabilities. Images (a–n) were created for this publication using the VMD 1.9.2 program<sup>[14]</sup> with some components and structures adopted from protein data bank entries (PDB ID: 4F5S, 4S05, 2L86), published models<sup>[15]</sup> and X-ray crystal structures.<sup>[16]</sup>

**Table 1.** Physical forces contributing to the interactions between biomolecules and AuNPs. Adapted with permission.<sup>[17d]</sup> Copyright 2013, Wiley-VCH Verlag GmbH & Co.

Forces	Strength	Net contribution	Range [nm] <sup>a)</sup>	Main factors
<b>Specific interactions</b>				
electronic/covalent	strong	large	<0.3	chemisorption vs physisorption to Au
π–π stacking	strong	large	0–5	aromatic ring orientation
salt bridges	strong	moderate	<1	multiple recognition
H-bonds	moderate	small	<0	donor/acceptor at interface
hydrophobic interactions	strong	large	0–10	hydrophobic functionalization
<b>Nonspecific interactions</b>				
vdW interactions	weak	large	0–10	Interface complementarity
Coulombic forces	moderate	moderate	0–10	charge state, ion strength

<sup>a)</sup>0 nm defined as vdW contact.

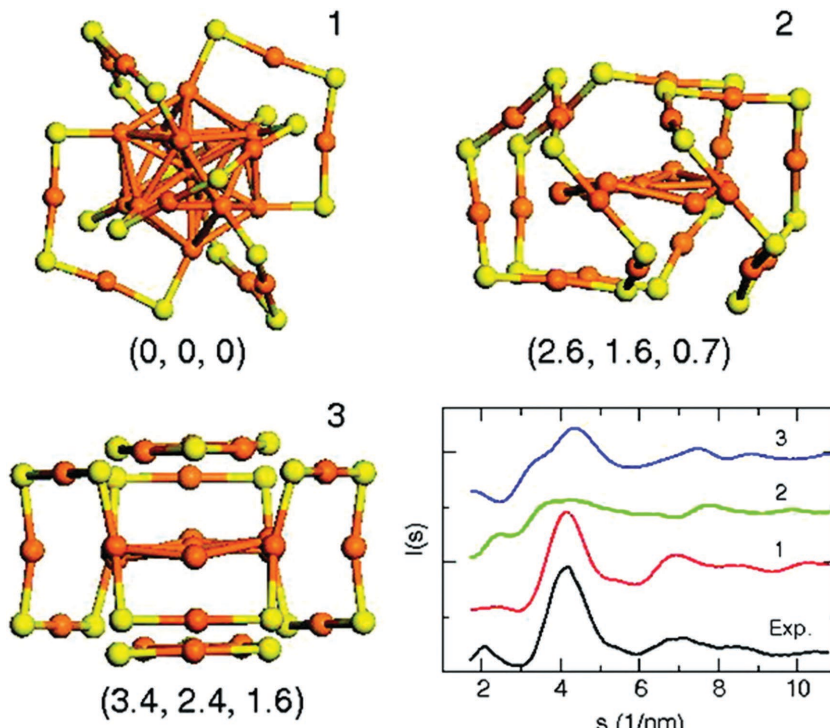


**Figure 2.** Optimized  $\text{Au}_{25}\text{Me}_{18}^-$  structure isomers (1–3) with the corresponding X-ray diffraction patterns compared to experiment. Gold atoms are colored orange, sulfur yellow, and methyl groups (Me) groups are omitted for clarity. Reproduced with permission.<sup>[24]</sup> Copyright 2008, American Chemical Society.

calculating and comparing the optical adsorption spectrum against experiment and as a complement to transmission electron microscopy (TEM) and small-angle X-ray scattering (SAXS) results.<sup>[23]</sup> For atomic configurations where there is little structural experimental data to compare to, empirical potentials (EP) have been employed as a first step in geometry optimization where first-principles calculations may

be prohibitively computationally expensive.<sup>[46]</sup> In their study of Au-Pd bimetallic NPs, Bruma et al. used a genetic algorithm at the EP level for a coarse exploration of configurational space, followed by a more accurate local optimization at the DFT level.<sup>[47]</sup>

As AuNC and AuNP structural information becomes more comprehensive, the capability to predict experimentally valid structures and enable the better understanding of the size-dependent physical and chemical properties of nanogold will assist the development of novel biologically relevant gold-based materials.

## 2.2. Mechanics of Nanoparticle Formation

In addition to static structure determination, QM methods may also be used to investigate the dynamics of AuNP formation, including aspects such as self-assembly/aggregation,<sup>[48]</sup> doping,<sup>[49]</sup> metal oxidation,<sup>[50]</sup> ligand exchange,<sup>[16a,39,51]</sup> and the binding of small molecules to gold surfaces<sup>[52]</sup> and nanoclusters.<sup>[53]</sup>

In a study of alkanethiol adsorption on AuNPs, Barnard observed that self-assembled monolayers form most favorably on the (111) facet adjacent to the (111)(111) edges, but alkanethiol concentration was the main determining factor in the differences in morphology.<sup>[54]</sup> Much work has also been done on the formation of Au-S staples, both for NPs<sup>[55]</sup> and surfaces.<sup>[56]</sup> The nature of the thiol bond has attracted significant literature debate, with some studies suggesting that gold atoms are formally

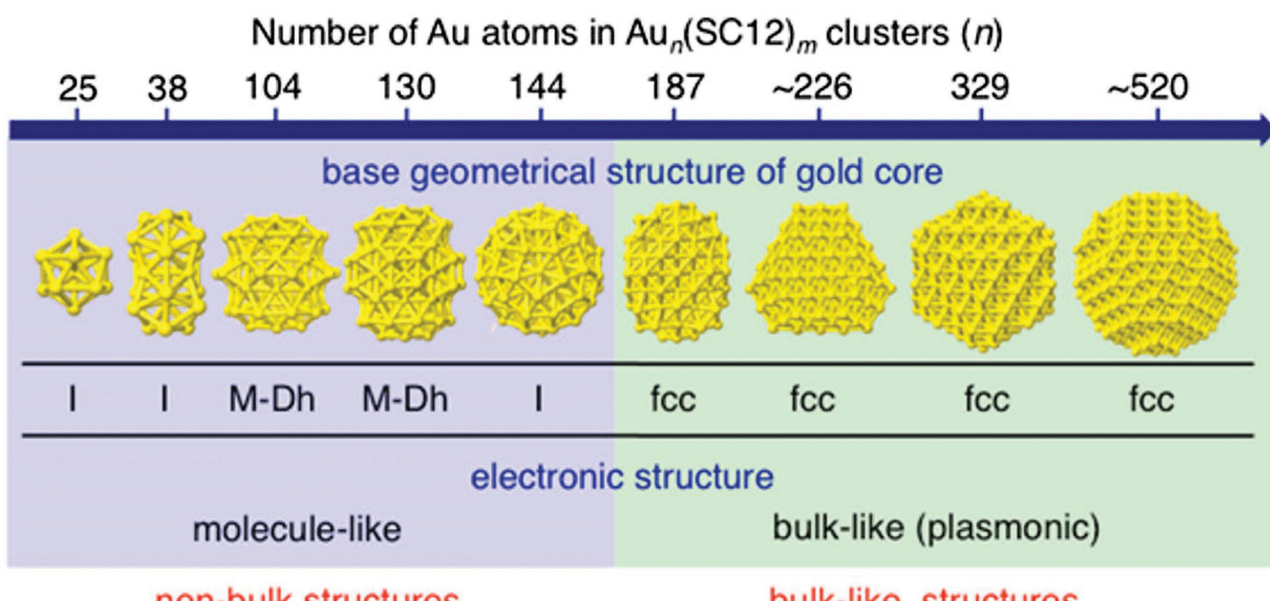


**Figure 3.** Transition from molecule-like to bulk-like electronic properties as a function of the number of gold atoms. Reproduced with permission.<sup>[37]</sup> Copyright 2015, American Chemical Society.

oxidized by the addition of thiols,<sup>[55a]</sup> while Reimers and others have suggested that the Au-S bond is predominantly covalent.<sup>[57]</sup> A recent review by Häkkinen covers this in excellent detail.<sup>[22c]</sup> DFT calculations have also provided insight in the effects of atomic substitutions,<sup>[58]</sup> chiral transfer,<sup>[59]</sup> adsorption-induced gold reconstructions,<sup>[60]</sup> and collocation of different adsorbents<sup>[61]</sup> on nanogold systems. Despite these accomplishments, understanding the precise mechanics of NP formation, specifically on the gold core itself, remains a challenge for ab initio methods due to the size/time scale limitations for this computationally expensive approach, although recent works have made great strides in this direction by considering the nucleation and growth process of small AuNCs at the QM level,<sup>[62]</sup> and by examining growth as a function of colloidal stability.<sup>[62a]</sup>

### 2.3. Optical and Electronic Properties

As one of the key biomedical applications for nanogold is biosensing,<sup>[6]</sup> an extensive understanding of the optical and electronic properties AuNPs exhibit as a function of their size is essential. The ability to functionalize AuNPs in order to fine-tune the optical and electronic properties and enable an optical response to biological stimuli is one of the characteristics that make AuNPs so attractive for theranostics.<sup>[6]</sup> QM calculations can aid this by enabling properties such as Highest Occupied Molecular Orbital-Lowest Unoccupied Molecular Orbital (HOMO-LUMO) gaps, photoinduced excitations, and electron transfer reactions to be studied in detail and as a function of atomic structure. Moreover, comparison of calculated absorption spectra to experimental absorption spectra can be used to validate proposed structures (as described in Section 2.1).

Time-dependent density functional theory (TDDFT) is an extremely useful method for calculating electronic excited states and properties associated with optical spectra.<sup>[63]</sup> Specific to AuNPs, multiple studies have used TDDFT to provide insight into the origin and nature of the optical properties of these systems. For example, Day et al. examined how the choice of DFT functional influences calculated electronic transitions.<sup>[64]</sup> Antonello et al. demonstrated that the oxidation state of the gold core affects the triple degeneracy of the HOMO in  $\text{Au}_{25}$ ,<sup>[65]</sup> while Tlahuice-Flores et al. found that distortion in the  $\text{Au}_{25}$  geometry reduces the HOMO-LUMO gap.<sup>[66]</sup> For the recently crystallized  $\text{Au}_{18}(\text{SR})_{14}$ ,<sup>[67]</sup> TDDFT shows that the HOMO extends over the staple, while the LUMO is on the core kernel, in contrast to other nanoclusters. Fihey et al. used a combined MD and QM approach to modify the  $\text{Au}_{25}$  ligand until excited-state charge transfer was possible (Figure 4).<sup>[68]</sup> They subsequently modified the ligand

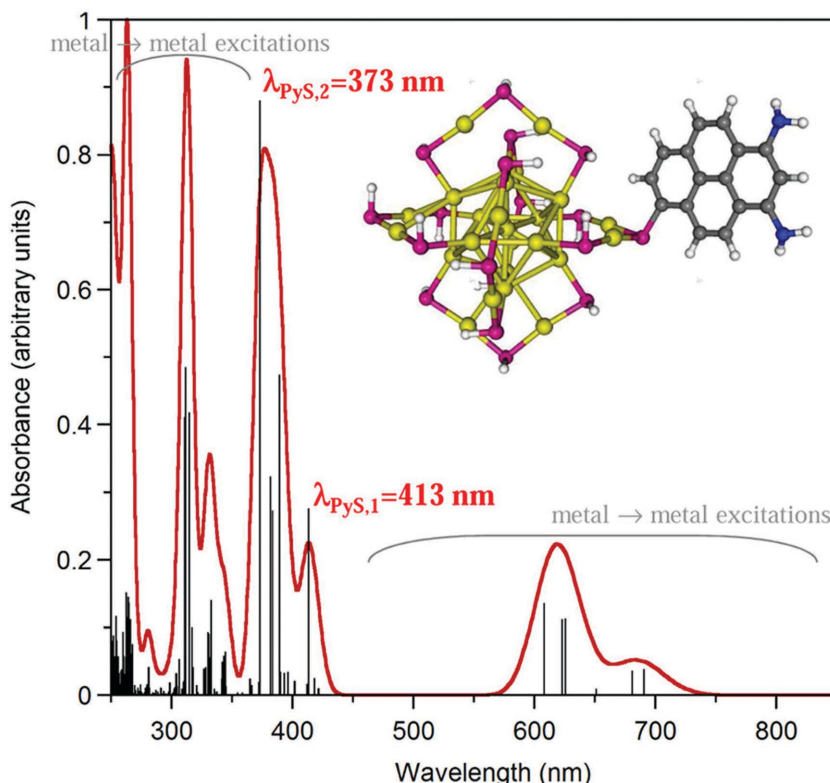


**Figure 4.** Detailed stick and convoluted absorbance spectrum of  $\text{Au}_{25}(\text{SH})_{17}\text{Py}(\text{NH}_2)_2\text{S}^-$ . Reproduced with permission.<sup>[68]</sup> Copyright 2014, American Chemical Society.

for electron transfer in order to form a molecular switch.<sup>[69]</sup> For larger AuNPs (>200 atoms), they employed a discrete interaction model in combination with TDDFT to accurately model surface plasmon resonance.<sup>[70]</sup> It is worth noting that while many TDDFT studies truncate the ligands for the sake of computational efficiency, Weissker et al. showed the importance of limiting truncation (e.g., shortening aliphatic chains to  $\text{CH}_3$  versus H) when comparing calculated absorption spectra to experimental spectra.<sup>[71]</sup>

Several studies have examined how atomic substitutions affect optical properties.<sup>[72]</sup> Muniz-Miranda et al. found that doping AuNCs with silver atoms increases the fluorescence quantum yield (observed experimentally) when a silver atom replaces the central position of the nanoclusters.<sup>[73]</sup> Pohjolainen et al. found that changing the ligand anchor atom had a pronounced effect on optical spectra.<sup>[74]</sup> Lugo et al. found by changing the chemistry of the ligand on different sized AuNCs that the more negative the partial charge on the core, the more the lowest absorption band was shifted to the red.<sup>[75]</sup>

While TDDFT is an exceptional method for examining the optical properties of NPs, it is not the only useful technique to do so. Tlahuice-Flores et al. found that far-IR and low-frequency Raman can be used to fingerprint AuNCs using standard DFT methods for calculating IR spectra.<sup>[76]</sup> Corni et al. used a novel approach to study the interactions between dye molecules and metal NPs by treating the metal NPs as a polarizable continuum and the dye molecules explicitly at the QM level of theory.<sup>[77]</sup> While QM techniques are extremely useful for examining optical and electronic properties of AuNPs, one of the key limitations is that fluorescence

emission spectra requires optimization of the excited state, which currently can only be achieved for small molecules.<sup>[78]</sup> However, this is only a limitation of the current computing power, and not a fundamental gap in the methodology.

## 2.4. Gold Interactions with Biomolecules

In general, the methods for investigating structure and optical properties of AuNPs are the same for both biological and non-biologically relevant systems. When QM calculations are employed specifically in the biological context, the focus is generally placed on the adsorption of biomolecules to the AuNP surface. In this context, both physisorption (accumulation of molecules on a surface without chemical binding) and chemisorption (covalent or ionic binding between molecules and the surface, i.e., functionalized gold) are considered. Physisorption is largely non-specific, but also may involve specific interactions such as hydrogen bonding and  $\pi$ - $\pi$  stacking. It is generally reversible, and dominated by van der Waals (vdW) forces with binding energies in the 2–10 kcal mol<sup>-1</sup> range per functional group. Chemisorption involves a chemical reaction between the molecule and the surface, and the binding energy can be a hundred times stronger.<sup>[79]</sup> Regardless of the type of adsorption, the proper treatment of weak dispersion interactions is critical.<sup>[80]</sup> Particularly with respect to the biological solvent, i.e., water, several studies have shown that the correct treatment of dispersion is required to properly model adsorption energy, binding orientation, and diffusion.<sup>[81]</sup> These studies have found that water molecules at gold surfaces tend to orient their oxygen atoms directly above a gold atom and closer to the Au interface than the hydrogen atoms, resulting in a tendency for interfacial water molecules to act as hydrogen bond donors.<sup>[81a,82]</sup>

Many biomolecule adsorption studies are used to parameterize FFs for the MM treatment of nano-bio systems where water is modeled explicitly (discussed in detail in Section 3).<sup>[82,83]</sup> Analogous studies have been done to derive gold biomolecular parameters for smaller nanoclusters.<sup>[84]</sup> In the development of the GolP-CHARMM FF,<sup>[82]</sup> Wright et al. utilized Plane Wave DFT (with the vdW-DF<sup>[85]</sup> to treat dispersion and revPBE<sup>[86]</sup> functionals) to examine the binding of small molecules representing the functional groups found in amino acids to the Au(111) and Au(100) surfaces. They found that with molecules containing sulfur or nitrogen, which chemisorb weakly to gold surfaces, there is a greater affinity for the Au(100) facet in vacuum. Although water is often treated implicitly or ignored altogether in QM calculations due to computational limitations, the correct treatment of water and understanding of water-gold interactions is essential. In the process of parameterizing the GolP FF,<sup>[83b]</sup> Hoefling et al. found a substantial difference between the DFT-derived orientations of amino acid building blocks and the geometries from MD simulations with an explicit solvent.<sup>[87]</sup> In a vacuum, the molecular orientations are driven by the attractive dispersion interaction and repulsive exchange term of the DFT functional, while in explicit solvent simulations the charged groups reorient for maximum exposure to water. In a separate study, Hong et al.

examined the interactions between several amino acids and the Au(111) surface in the presence of water molecules and found that charged residues bind more strongly to the gold surface due to charge transfer, and tuning pH could potentially change the binding affinity.<sup>[88]</sup>

Apart from biomolecules on gold surfaces, other studies have looked at the interactions between a small number of gold atoms and amino acids such as cysteine<sup>[89]</sup> and glycine.<sup>[90]</sup> For individual amino acids interacting with small AuNCs, Pakiari et al. found that anionic amino acids were favored.<sup>[91]</sup> Similar results were found for the tripeptide glutathione,<sup>[92]</sup> which is an alternative capping ligand to alkanethiolates for AuNC nano-bio applications. In their QM/MM study of Au<sub>25</sub> functionalized with glutathione, Rojas-Cervellera et al. demonstrated that the proper treatment of both ligand and solvent effects was necessary to accurately model both structural and optical properties of the AuNC, and previous calculations on HOMO-LUMO gaps appeared accurate due to a cancellation of errors.<sup>[93]</sup>

In addition to amino acids, the interactions of nucleobases with gold surfaces<sup>[83a]</sup> and small clusters<sup>[94]</sup> have also been investigated. A recent DFT study found the trend in the interaction between nucleobases and small AuNCs followed the order of G > A > C > T > U.<sup>[95]</sup> Moreover, Rai et al. found that AuNCs can also alter the properties of DNA base pairs.<sup>[96]</sup>

While there have been simulations using ab initio MD to study AuNPs on the picosecond time scale,<sup>[97]</sup> for an examination of entropic effects in physiologically meaningful (solvated) systems, other methods must be used.

## 2.5. Large-Scale QM Techniques

For larger NPs and longer time scales, where conventional DFT becomes prohibitively computationally expensive, simplified QM approaches such as tight-binding (DFTB)<sup>[98]</sup> and other semi-empirical methods<sup>[99]</sup> play a valued role. Over the last few decades, the development of linear-scaling  $O(N)$  methods such as ONETEP<sup>[100]</sup> and SIESTA<sup>[101]</sup> have become significant tools for studying large systems at the electronic level. The key feature of these methods is their computational efficiency obtained by exploiting the inherent locality or “near-sightedness” of the single-particle density matrix in many systems, while retaining accuracy akin to traditional plane-wave basis set codes. Such efficiency opens up the possibility of performing accurate DFT calculations on systems with thousands and tens of thousands of atoms, including nanomaterials,<sup>[102]</sup> proteins,<sup>[103]</sup> and more complex/conjugated systems such as NPs interfaced with complete proteins<sup>[104]</sup> and gold/thiolate molecular junctions.<sup>[105]</sup> Linear-scaling techniques have also been used as complement to classical MD simulations for further DFT-based structure refinement and binding energy determination.<sup>[104,106]</sup> For example, in a recent investigation of the self-assembly process of cysteines on a reconstructed Au(110) (1 × 2) surface, there was disagreement between SIESTA DFT calculations and MD simulations (with centrosymmetric potentials),

with the FF approach maximizing the coordination of the adsorbate groups and ignoring the differences in reactivity of various Au sites.<sup>[106]</sup> This demonstrates the importance of FF parameterization for non-uniform surfaces.

QM/MM methods are also useful for investigating large complex systems, where the electronic properties of a selected region are described at the QM level and the surrounding environment described at the MM level.<sup>[93,107]</sup> A challenge of this method is the uncertainty in how to define these two (or more) regions, which will ultimately affect the accuracy of the results, especially if the QM region is not large enough or the interface between the QM and MM regions is not modeled accurately. It is evident that DFT calculations on entire (or at least sufficiently large regions of the) complex biological systems are impractical thus providing an avenue for linear-scaling DFT methods to fill this expanding gap.

### 3. All-Atom Molecular Mechanics and Dynamics (Force Field Methods)

The complexity and size of gold–bio systems that contain inorganic, biomolecule, ionic and aqueous species quickly renders even linear-scaling QM techniques computationally intractable for simulation times approaching the nanosecond-scale. Furthermore, the common workaround to increase QM system size by neglecting solvent effects is less than ideal, as these effects are well known to play an active role in biological processes.<sup>[108]</sup> There is thus a need to complement enthalpically driven QM calculations with a description of the system's free energy that includes both the enthalpic and entropic contributions. This can be achieved through methods based on classical statistical mechanics, where thermodynamic properties of AuNP–bio systems can be investigated in physiological environments and at an appreciable level of accuracy without compromising computational efficiency.

#### 3.1. The Potential Energy Function

Molecular mechanics involves describing inter-atomic interactions as “classical” or physical processes through an analytical expression called a force field. Used to calculate the total potential energy ( $V^{\text{tot}}$ ) of a molecular system, a common functional form of a FF is:

$$\begin{aligned} V^{\text{tot}} = & \sum_{\text{bond}} K_b (b - b_0)^2 + \sum_{\text{angle}} K_\theta (\theta - \theta_0)^2 \\ & + \sum_{\text{torsion}} K_\varphi [1 + \cos(n\varphi - \delta)] \\ & + \sum_{\text{LJ}} 4\epsilon_{ij} \left[ \left( \frac{\sigma_{ij}}{r_{ij}} \right)^{12} - \left( \frac{\sigma_{ij}}{r_{ij}} \right)^6 \right] \\ & + \sum_{\text{Coulomb}} \frac{q_i q_j}{4\pi\epsilon_0 r_{ij}} + \sum V^{\text{other}} \end{aligned} \quad (1)$$

Each term in Equation (1) describes the energetic contributions associated with a specific type of inter-atomic interaction and is composed of a function and corresponding parameters (empirically and/or theoretically determined). The first two terms describe covalent bond stretching and angle bending using relatively simple harmonic functions (Hooke's Law) with force constants  $K_b$  and  $K_\theta$  defining the strength of the energetic penalty imposed for deviations of the bond length ( $b$ ) and angle ( $\theta$ ) from defined minimum energy positions ( $b_0$  and  $\theta_0$ , respectively). The torsion term uses a periodic function to model how varying the dihedral angle ( $\varphi$ ) between atoms separated by 3 covalent bonds affects the potential energy with respect to the potential barrier to rotation ( $K_\varphi$ ), periodicity ( $n$ ), and phase ( $\delta$ ). Non-bonded atom pair interactions are described as functions of the separation distance  $r$  between the centers of particles  $i$  and  $j$ . Close-range repulsion and vdW dispersion interactions are represented by a Lennard-Jones (LJ) 12–6 potential where  $\sigma_{ij}$  and  $\epsilon_{ij}$  are the finite distance at which the inter-atomic LJ potential is zero and the potential well depth, respectively. Electrostatic interactions are treated via Coulomb's law where  $\epsilon_0$  is the permittivity of free space and  $q_i$  is the partial charge assigned to each atom. Finally, the last term of Equation (1) encompasses all other “FF specific” interactions that may feature, such as coupling between terms, out-of-plane bending, induced polarization (see Section 3.2), external applied forces, etc. It is primarily the availability and quality of a FF's parameters that reflect how accurately inter-atomic interactions (and subsequently physical phenomena) are emulated in silico. Although well-established biological FFs (e.g., AMBER,<sup>[109]</sup> CHARMM,<sup>[110]</sup> GROMOS<sup>[111]</sup> and OPLS/AA<sup>[112]</sup>) have been developed and validated over several decades to reproduce basic biomolecular properties, they lack the parameters necessary for investigating biomolecule behavior in gold-containing systems. Due to gold's innate chemical inertness, most species (excluding thiols, see Section 2.2) primarily physisorb to gold, therefore extending conventional biological FFs to capture this interaction mainly requires reliable gold–organic vdW parameters and atomic charges (see Section 2.4). Many FFs handle vdW interactions through a LJ potential, commonly in the 12–6 form (Equation (1)).

By incorporating tailored gold-specific LJ parameters (i.e.,  $\sigma_{ij}$ ,  $\epsilon_{ij}$  where  $i = j = \text{Au}$ ) for various Au surface facets and cluster geometries into an existing FF's functional form, the interaction energy between gold and other atom types can be estimated. This is done through assuming the validity of standard mixing/combination rules, such as  $\sigma_{ij} = (\sigma_i + \sigma_j)/2$  and  $\epsilon_{ij} = (\epsilon_i \times \epsilon_j)^{1/2}$ , which are already established approximations within the biological FFs themselves. Yet as highlighted by Latour,<sup>[113]</sup> parameters derived to represent biomolecule-solution interactions should not automatically be assumed to be directly transferable to biointerfacial systems. With this in mind, the only viable approach to modeling AuNP–bio interfacial systems is through developing parameters (in a consistent way) to be both specific for particular Au nanostructures or surface facets and compatible with extensively tested bio-organic FFs. Ideally, further developments of gold–bio FFs would be done in conjunction with experimental data. However, at this moment, there is little, if any, useable experimental data available for this purpose. While some adsorption experiments of small molecules and synthetic peptides have

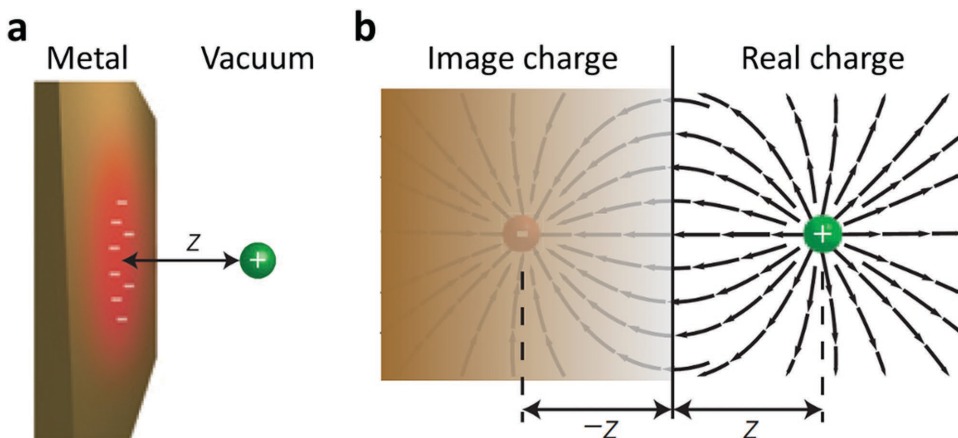


**Figure 5.** Schematic illustrating the concept of induced polarization. a) A positive charge at a close proximity to a metal surface induces a negative charge at the surface. b) Electric field produced by the point charge outside the metal, with field lines shown by arrows. Reproduced and adapted with permission.<sup>[115]</sup> Copyright 2013, Nature Publishing Group.

already been specifically designed and used for validation of non-bond interaction potentials,<sup>[114]</sup> at the present stage QM calculations are filling the parameterization gap.

### 3.2. Polarizability

It is worth mentioning that due to the metallic nature of gold (especially surfaces), it is desirable, from a physical perspective, to explore the interactions solvent and solute molecules have with the polarization they induce in the metal (also known as image charge effects, **Figure 5**). Image effects not only create an attractive interaction between charges and metals, but they can also affect mutual interactions between charges in adsorbed molecule(s).

Although not all classical FFs for metal-molecule interactions explicitly include polarization terms in their functional form, some effects might still be implicitly included in the remaining two-body metal-molecule parameters, depending on the parameterization approach (e.g., QM approaches where polarization is intrinsic). Nevertheless, since many biomolecules invariably feature charged domains, polarization effects are generally not negligible. Therefore, the incorporation of explicit, on-the-fly, polarizability for gold atoms in classical simulations would be ideal. A few dynamic models currently implemented for this purpose include the rigid-rod approach of Iori and Corni,<sup>[116]</sup> and more recently the capacitance-polarizability interaction model, which also allows an atomistic description of charge migration within a particle.<sup>[117]</sup> Other a posteriori methods to quantitatively measure facet-dependent polarization effects have also been published in the literature,<sup>[118]</sup> however these carry the limitation that the atomic positions cannot respond to the image potential (see discussion given in [119]).

### 3.3. Tailored Gold–Biomolecular Force Fields

When FFs are developed they are usually designed with a specific application in mind and aim to explicitly reproduce

some characteristic of a particular atomic system as a validation step. This focus may be ensuring that the crystal structure of a small AuNCs is maintained, or verifying that the experimental interaction energies and adsorption geometries of molecules onto different gold surface facets are adequately reproduced. Although there is no “one size fits all” FF capable of replicating the complex physicochemical phenomena at the gold–bio interface, currently there are two conceptually different mainstream approaches commonly taken when constructing gold–biomolecular FFs. One approach is targeted at general and transferable interfacial gold-specific parameters capable of modeling any shaped gold material as well as reconstruction of the substrate within one comprehensive framework. The alternative approach introduces a number of tailored parameters aimed at differentiating the interactions between particular biomolecular species and different crystallographic facets and shapes of gold, while keeping the geometry of gold substrate/center rigidly intact. For detailed description of both methods and validation data please refer to the discussions found in [120] and [121], and references therein. Herein we give a general account of both approaches, as well as others, used in developing custom FFs able to represent the interactions occurring between gold (surfaces/clusters) and biomolecules (water/ligand/protein/DNA). As with all simulation work, there is currently no single “best” method to model gold, and the best approach for a particular system is the one that most accurately reproduces the properties of interest.

#### 3.3.1. Lennard-Jones Gold Particles

Possibly the most “transferable” and hence popular gold LJ parameters are those of the METAL/INTERFACE FF of Heinz et al.,<sup>[12,122]</sup> which were developed to reproduce the experimentally measured bulk density and surface tension of homoatomic face-centered cubic (FCC) metals. Available as 12–6 and 9–6 LJ parameter sets,  $\sigma_{\text{Au,Au}}$  and  $\epsilon_{\text{Au,Au}}$  are claimed to be compatible with a wide-range of “organic” FFs such as AMBER,<sup>[109]</sup> CHARMM,<sup>[110]</sup> OPLS/AA,<sup>[112]</sup> COMPASS,<sup>[123]</sup> and CVFF.<sup>[124]</sup> The universal applicability with so many FFs

is reasoned to be a result of the parameter validation process only involving properties of pure gold and non-bonded interactions, ultimately leading to different FFs yielding the same metallic density and surface tension. The LJ description of gold in the METAL/INTERFACE FF allows for the classical Hamiltonian energy expression to reproduce the FCC structure and surface energy of gold which leads to a good agreement of the calculated metallic thermal and mechanical properties with experimental values.<sup>[12]</sup> Furthermore, the authors assert that it is these surface and interface properties of metals that dictate the interactions with other components (e.g., biomolecule species), which enhances the applicability of the parameter set to interfacial systems.

While the gold atoms in this FF are charge-neutral, they are not geometrically restricted, allowing for the exploration of molecules interacting with different crystallographic surfaces,<sup>[125]</sup> faceted and spherical AuNPs,<sup>[126]</sup> as well as other shaped gold constructs.<sup>[127]</sup> Polarization is not described explicitly, but polarization effects were quantitatively tested a posteriori and found to contribute up to  $\approx 20\%$  of the binding energy for highly charged biopolymers on the Au(111) surface, while for other surfaces such as the Au(100) the contribution from polarization is more significant or even dominant.<sup>[118]</sup> Peptide/protein binding to Au(111) using the METAL FF is described as a “soft epitaxy” type mechanism, with adsorption via the surface’s hollow sites,<sup>[128]</sup> which is (albeit indirectly) supported by experimental studies showing near perfect epitaxial ordering of alkanes and some amino acids at monolayer coverage on Cu(111) and Pt(111) surfaces. Alternative hypotheses suggest that it is interfacial water structuring rather than epitaxy that plays a critical role in peptide-gold binding.<sup>[129]</sup> It should also be mentioned that as a result of solely relying on LJ terms to maintain gold atoms in the desired FCC morphology, the depth of the LJ potential well is relatively large (12–6:  $\epsilon_{\text{Au},\text{Au}} = 19.1 \text{ kJ mol}^{-1}$ ) since it represents strong cohesion. Although this raises concerns about overestimating the strength of vdW interactions between mixed species, computed water and peptide adsorption energies using the METAL FF are in agreement with experiment.<sup>[130]</sup> Furthermore, the recently published thiolated nanocluster FF of Guberman-Pfeffer et al.<sup>[131]</sup> also features similar magnitude  $\epsilon$  values for gold atoms. For further details and benchmarking we refer the reader to the most recent extensive review.<sup>[120]</sup>

Besides the METAL FF, several other sets of LJ parameters have been used to model bio-gold systems while relying on cross-terms to govern gold’s interactions with organic and biomolecular components.<sup>[106,132]</sup> These include the hydrophilic parameters of Vila Verde,<sup>[133]</sup> parameters borrowed and modified from the generic Dreiding<sup>[134]</sup> and universal<sup>[135]</sup> force fields, parameters adapted from experimental data,<sup>[136]</sup> and those taken from self-assembled organic monolayers on gold substrates.<sup>[137]</sup> It is worth noting that due to the nearly ubiquitous nature of thiolates in AuNP-bio systems, it is often necessary to accurately and explicitly represent the Au-S bond (e.g., found between deprotonated cysteine and Au) within the simulation protocol. There have been many examples in the literature where harmonic potentials,<sup>[138]</sup> Morse potentials<sup>[132a,139]</sup>

and various strong short-range potentials<sup>[106,140]</sup> have been appropriately used to reproduce this bond for specific applications. However, as adhesion of many biomolecules (such as proteins) to gold is known to be largely dominated by secondary interactions, standard mixing rules may fail to accurately describe the varying physicochemical strength of interaction different atom types have with gold. This issue has been a strong motivator behind the also popular GolP family of FFs.<sup>[82b,83b,84b,121,141]</sup>

### 3.3.2. Peptides and Proteins

The GolP FF was designed to examine how proteins interact with gold surfaces, initially the (111) facet.<sup>[83b]</sup> It was parameterized against both QM and experimental data to reproduce adsorption geometries and interaction strengths of natural amino acids on this gold facet. Although interactions between gold and other atomic species are still governed by 12–6 LJ potentials, GolP additionally introduces explicit “Au-X” LJ terms to ensure weakly chemisorbed sulfur- and nitrogen-containing molecules (imidazole, NH<sub>3</sub>, CH<sub>3</sub>SH and CH<sub>3</sub>SCH<sub>3</sub>) and  $\pi$ -conjugated species are correctly described. Furthermore, two unique features of the GolP FF are the inclusion of LJ virtual sites to constructively direct the geometry of biomolecule adsorption (as obtained from DFT calculations), and the use of a rigid-rod dipole method<sup>[116]</sup> to dynamically and efficiently describe induced gold polarization. This method to treat polarization is qualitative, empirical in nature, i.e., sacrifices the realism of a quantum description, and does not allow for charge accumulation to develop on the metal. However, the inclusion of polarization effects is not only beneficial for the reasons discussed in Section 3.2, but also because this potentially enables the transferability of gas-phase derived parameters to the condensed phase, as demonstrated by the polarizable AMOEBA FF.<sup>[142]</sup>

The GolP Au(111) surface is represented as a 5-layer periodic slab in 2 dimensions with gold atoms holding no partial atomic charge and no intra-surface (i.e., gold-gold) parameters. As a result, the gold atoms must be kept rigid in their equilibrium position, which disables any potential gold lattice deformations and removes the ability of the FF’s Hamiltonian to compute metallic surface energies or describe nanocrystal growth, thermal properties, or mechanical properties of the metal. However, for studying gold surface-biomolecular interfaces this is an acceptable approximation, considering the much stronger cohesion of gold relative to soft matter. GolP was developed to be compatible with OPLS/AA<sup>[143]</sup> and will henceforth be referred to as GolP-OPLS here.

To address the facet-selectivity of peptide adsorption, Wright et al. reparameterized GolP-OPLS with the CHARMM FF<sup>[110,144]</sup> and extended it to describe both the Au(111) and Au(100) surface facets, which are the most common facets of relatively large (approx.  $> 3 \text{ nm}$ ) AuNPs.<sup>[145]</sup> Termed GolP-CHARMM,<sup>[82]</sup> the FF analogously features virtual sites and dynamic polarization and introduces explicit LJ terms to reproduce the energetics and structuring of water at gold surfaces, an important aspect for biological applications.

In a further extension, the GoLP-CHARMM FF was expanded to describe reconstructed Au(100)-hex surfaces, approximated as (1×5).<sup>[121]</sup> Although experimental evidence shows that both Au(111) and Au(100) are present in their reconstructed forms in biologically relevant conditions,<sup>[146]</sup> only Au(100)-hex shows significant structural differences from its unreconstructed counterpart Au(100)(1×1). Using MD simulations with GoLP-CHARMM, the authors highlighted that this surface reconstruction cannot be ignored as differences in water structuring at the native and reconstructed Au(100) interfaces led to significant discrepancies in peptide binding affinities.<sup>[121,129]</sup>

Even though it is essential to understand how molecules interact with gold in a fully explicit aqueous environment, for some applications this level of treatment prohibits the user from investigating the behavior of large biomolecular systems and long time scale phenomena. For these purposes, implicit solvent methods such as the ProMetCS model<sup>[141b]</sup> offer a computationally efficient approach to atomistically model protein-Au(111) interactions while approximating the solvent to a continuum.

### 3.3.3. DNA and RNA

It is also significant to acknowledge that alongside proteins and peptides, DNA/RNA molecules represent a major class of biomolecules that are increasingly being incorporated into many gold-based assays. For example, to detect the presence and concentration of DNA or proteins in solution, single-stranded DNA (ssDNA) can be attached to AuNPs as a probe molecule.<sup>[1b]</sup> Unlike conventional double-stranded DNA (dsDNA) which consists of hydrophilic outer backbones and hydrophobically protected inner nucleotide base pairs, ssDNA molecules are completely solvent exposed, leading to very different behavior in water and ultimately at the AuNP-interface. To capture this at the classical level, Jiang et al. developed a modified AMBER03 FF<sup>[147]</sup> for ssDNA interacting with Au(111) and preliminary testing has demonstrated good correlation with experimental data.<sup>[148]</sup> A similar approach was taken by Mudedla et al. for siRNA.<sup>[149]</sup> As nucleic acids in standard biological FFs are parameterized to reproduce the solution properties of dsDNA, new QM-based natural bond order (NBO) atomic charges were derived for each nucleobase to ensure an accurate representation of ssDNA's physics and hydrophobicity, which are significantly different from dsDNA. Similarly to the FFs mentioned in Section 3.3.1, the uncharged atoms on the Au(111) surface are described as LJ particles ( $\sigma_{\text{Au,Au}} = 0.29 \text{ nm}$ ,  $\epsilon_{\text{Au,Au}} = 0.43 \text{ kJ mol}^{-1}$ ) with mixing rules dictating Au–ssDNA interactions.

Despite the emergence of ssDNA–gold devices in the literature, the interaction of dsDNA with gold is still of paramount importance. Therefore, a GoLP-like FF called GoldNA-AMBER was designed to reproduce dsDNA interactions with Au(111) surfaces.<sup>[141a]</sup> Consistent with GoLP-OPLS and GoLP-CHARMM, the FF features virtual sites, dipolar rigid-rod polarization and optimized water–gold interaction parameters. However, biomolecular compatibility was shifted to the AMBER FF due to its reliable description of dsDNA in solution.<sup>[150]</sup>

### 3.3.4. Thiolated AuNCs

Unlike gold surfaces and faceted NPs, small thiol-protected AuNCs (introduced in Section 2.1) display a very different atomic arrangement from that of the well-recognized FCC lattice. Instead, these small AuNCs (approx. < 3 nm) exhibit X-ray crystal structures that contain highly symmetric gold cores, surrounded by adatom “staples” (Figure 2). Within this small size regime, capturing the quantum chemical nature (no longer bulk metal band structuring) and vastly different morphology of AuNCs presents a significant FF design challenge for classical all-atom molecular simulation. This is primarily due to limited availability of experimental data and how recently they have been chemically characterized, which is reflected by the fact that only very few all-atom (staple motif containing) thiolate-AuNC FFs have appeared, namely for  $\text{Au}_{25}(\text{SR})_{18}$ ,<sup>[84,151]</sup>  $\text{Au}_{38}(\text{SR})_{24}$ <sup>[84a,152]</sup> and  $\text{Au}_{144}(\text{SR})_{60}$ .<sup>[153]</sup> Within these FFs, gold can be designated different atom types depending on the coordination to metallic and/or ligand atoms (i.e., Au–Au–Au, Au–Au–S or S–Au–S).<sup>[84]</sup> This allows for interaction parameters to be optimized for each gold type much like different atom types are treated in biological FFs. Similar to many atomistic surface FFs, gold atoms may be neutral<sup>[151a]</sup> or have assigned charges,<sup>[153a]</sup> and either be forced to occupy their equilibrium positions (restricting intra-gold interactions and removing the need for Au–Au parameters)<sup>[151a]</sup> or allowed to evolve under a fully parameterized Au–Au FF<sup>[84b]</sup>.

While a primary parameterization goal for these FFs is to maintain the internal AuNC morphology of an experimental crystal structure, this only applies to the Au and S atoms, and the exploration of the ligand-conformational energy landscape is of prime importance. This is highlighted by Ouyang and Jiang, who fixed the Au and S atoms to their experimental positions and found that many ligand conformations of  $\text{Au}_{25}(\text{SC}_2\text{H}_4\text{Ph})_{18}$  were at a lower energy than that of the crystalline state.<sup>[151b]</sup>

Recently, GoLP-OPLS compatible parameters for  $[\text{Au}_{25}\text{S}(\text{CH}_2)_2\text{Ph}]^{-1}$  were developed to investigate how small hydrophobic AuNCs interact with proteins, which for the purposes of this review we will term the GoLP-OPLS-Au<sub>25</sub> FF.<sup>[84b]</sup> Bond parameters for Au–Au, Au–S and S–C atom pairs, as well as the corresponding bond angles, were established based on extensive ab initio calculations and validated against the experimental  $[\text{Au}_{25}(\text{SR})_{18}]^{-1}$  crystal structure. Charges for gold and organic atoms were also derived in addition to LJ parameters fitted to replicate the QM interaction of (an OPLS) methane molecule with the AuNC.

### 3.3.5. Reactive FFs

Reactive FFs such as ReaxFF (originally developed for hydrocarbons)<sup>[154]</sup> allow for bond formation and cleavage to be updated “on the fly” during MD simulations and as such can be used to model chemical reactions like gold surface reconstructions upon thiolation.<sup>[155]</sup> In 2008, ReaxFF parameters for gold<sup>[156]</sup> were developed and subsequently expanded to describe Au–S–C–H systems.<sup>[155,157]</sup> More recently, a modified version of ReaxFF has been applied

to study the binding mechanism of cysteine to gold, which confirmed the experimentally determined two-step binding process of an initial slow physisorption followed by a fast chemisorption and the formation of the “staple” motif.<sup>[158]</sup> Although reactive FFs provide accuracy approaching QM methods at a substantially reduced computational cost, the rigorous parameterization needed to extend the ReaxFF framework has limited its applicability to model larger and physiologically relevant systems. Further limitations in the charge equilibration calculation model and description of dispersion interactions within the ReaxFF framework are discussed in reference.<sup>[159]</sup>

#### 4. Coarse-Grained and Simplified Approaches

As is the case with all molecular simulation problems, as the number of atoms and time scale of the physicochemical phenomena of interest increase, so too does the computational demand, hindering the use of all-atom techniques to comprehensively investigate large-scale events such as NP aggregation or membrane permeation. Instead, to probe the spatial and temporal resolutions needed for these biomolecular processes/events, atomistic models can be complemented with lower-resolution coarse-grained (CG) methods that use groups of atoms as single interaction sites (or “beads”). This allows for both a reduction in the system’s degrees of freedom as well as the utilization of larger integration time steps (tens of femtoseconds) and makes CG models at least two to three orders of magnitude faster than analogous all-atom simulations. The development and design of CG models and FFs, largely require the careful consideration of three things: the particle mapping strategy, the type of interaction potentials, and their parameterization and validation, which are discussed below.

First, an atomistic structure of interest must be transformed (or mapped) to a CG representation. During this process, molecular regions of chemical or structural importance are able to be prominently represented and distinguished in the CG model whereas insignificant domains can be ignored. Also, depending on the “coarseness” of the mapping, flexibility or rigidity can be introduced to different parts of the model and computational efficiency can be tailored as required. Irrespective of the mapping approach, it is especially important to ensure the level of atomic detail sacrificed does not compromise the structural and dynamic properties of interest in the system. Once an appropriate representation has been established, the types of interaction potentials employed between CG sites must be determined. These may range from simple potentials such as those seen in classical all-atom FFs (i.e., weak-harmonic, LJ and Coulomb potentials – see Equation (1)), to much more complex CG potentials containing many-body terms (see [160] and references therein). Finally, the CG interaction potentials must undergo parameterization and validation, i.e., FF parameters are fine-tuned to reproduce experimental data (top-down or thermodynamic-based approach),<sup>[161]</sup> and/or extracted from high-quality reference atomistic simulations (bottom-up or structure-based approach).<sup>[162]</sup>

Through these general procedures, many biomolecular CG FFs have been established that treat elements such as proteins, lipids, nucleic acids, and water in diverse ways.<sup>[160,161]</sup> For example, one of the most common and widely used CG approaches that maintains chemical distinction between the building blocks of a biomolecule (such as the backbone and side-chain of a protein) is the MARTINI FF.<sup>[163]</sup> Developed for lipids, proteins and, more recently, DNA,<sup>[163,164]</sup> the MARTINI FF was originally parameterized to reproduce the experimental partitioning free energies of individual amino acids through lipid bilayers, and has also been used to describe nano-bio interactions, NPs and polymers for self-assembling systems.<sup>[164a]</sup> A major drawback of the current MARTINI FF (for proteins) is that it relies on a folded structure reference therefore it is unable to realistically model secondary structure evolution. Other CG techniques have recently been designed that advantageously do not require a priori knowledge of the secondary structure, however have a greater degree of coarseness (one amino acid per bead) and lack chemical residue identity.<sup>[165]</sup> Over the past few years we have also seen the emergence of hybrid MD simulations where the environment has been coarse-grained while the solute has been atomistically treated (AA/CG models), which have been shown to be both computationally efficient and sufficiently accurate for biomolecular simulations.<sup>[166]</sup>

In any CG technique, there is a compromise between the lack of detail and the properties that are being sampled. The application of a given CG FF is largely determined by the focus of the work and the properties of the system under study. It is outside the scope of the current work to extensively discuss the many approaches, models, technical aspects, opportunities and challenges associated with general CG biomolecular simulations, interested readers are referred to the following excellent recent reviews<sup>[160–162]</sup> and references therein.

In the context of CG AuNP-bio systems, it is particularly important to acknowledge that for many biomedical applications such as drug delivery, AuNPs are used as carrier entities to transport other molecules into the interior of a cell while the functional layer on the gold surface dictates the NP’s interactions with the environment.<sup>[3]</sup> As such, depending on the context of the application of interest, it is often justified to neglect a significant amount of detail when describing AuNPs in CG simulations. For example, entire AuNPs can be approximated as a single LJ particle<sup>[167]</sup> (Figure 1k and l) or as an effective field,<sup>[168]</sup> small groups of gold atoms can be mapped to single beads (4:1)<sup>[169]</sup> (**Figure 6a**), or AuNPs can retain all atomistic structure with each gold atom treated as a LJ bead (1:1 mapping).<sup>[170]</sup> Other noteworthy simplified approaches (although otherwise atomistic) involve neglecting some or all of the gold atoms that make up the metallic core of monolayer-protected AuNPs. In these models the “missing” Au mass is redistributed to either the surface gold atoms (in hollow, spherical NP models, Figure 6b)<sup>[171]</sup> or the ligand sulfur atoms (for models where gold is implicit).<sup>[172]</sup>

A lot of interest within the CG community is aimed at modeling AuNP translocation through cellular membranes<sup>[170a,c,173]</sup> and the NPs themselves can either be bare<sup>[173]</sup> or coated with various ligands such as

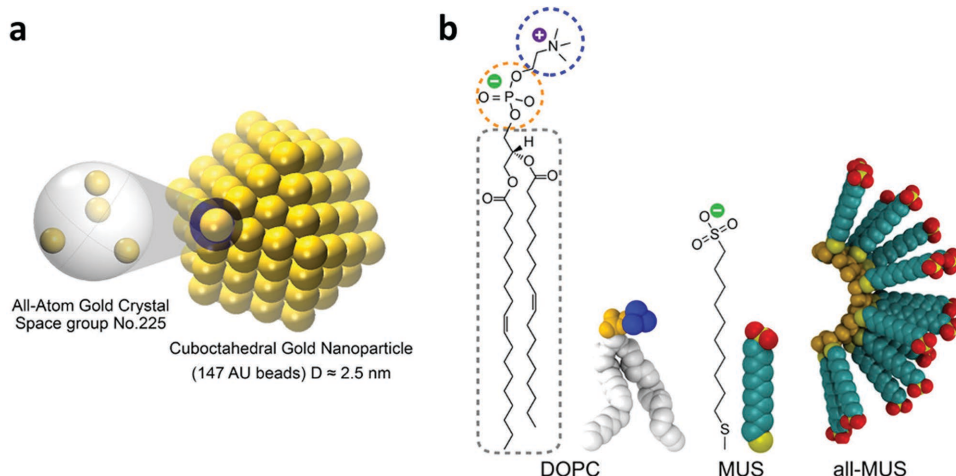


**Figure 6.** CG models of AuNPs illustrating some approaches to coarse-graining. a) 4:1 mapping of a faceted NP. Reproduced with permission.<sup>[169a]</sup> Copyright 2014, American Chemical Society. b) chemical structure of lipid and hollow AuNP, respectively. Adapted with permission.<sup>[171b]</sup> Copyright 2014, American Chemical Society.

alkanethiols,<sup>[170a,c,e,173b]</sup> polymer brushes,<sup>[169a]</sup> peptides<sup>[170b]</sup> or a mixture of hydrophobic and hydrophilic ligands.<sup>[168]</sup> Others have investigated the interaction of proteins with citrate-capped AuNPs<sup>[167]</sup> and the aggregation of alkanethiol-AuNPs.<sup>[169b,170]</sup> Regardless of the description of gold, often the scale-up is realized from the CG treatment of non-gold components such as ligand molecules, lipid bilayers and solvent, as they normally constitute a larger portion of the system. Also care must be taken to ensure that the gold parameters are fully compatible with the rest of the CG FF in a meaningful and realistic way and that a consequence of the reduction in the degrees of freedom, validation of CG simulation results and other simplified models (such as dissipative particle dynamics<sup>[174]</sup>) is crucial to ensure the essential features necessary to adequately describe the chemistry and physics of the processes of interest are still present.

## 5. Enhanced Sampling Techniques

Extraction of realistic kinetic and thermodynamic quantities from gold–bio interface simulations requires a thorough and comprehensive sampling of the potential energy landscape. For complex systems this free energy profile is characterized by multiple low energy metastable states separated by high energy barriers. Classical (brute-force) MD simulations can often fail to cross high energy barriers and sample rare events due to the inherent femtosecond integration time steps and limited simulation times. Therefore, as with other systems incorporating highly flexible molecules, it is necessary to employ techniques capable of robust sampling of the conformational space to obtain a statistically representative depiction of the system's behavior. Some of these techniques include umbrella sampling,<sup>[175]</sup> metadynamics,<sup>[176]</sup> “replica-exchange” based techniques,<sup>[177]</sup> and approaches based on performing exhaustive multiple independent MD simulations starting from different initial orientations, structures and/or velocities.<sup>[178]</sup>

Several comprehensive reviews on the advancement and need of enhanced sampling techniques have recently appeared.<sup>[113,179]</sup> Through the development of advanced sampling simulations techniques, along with the increase in computational power, rigorous conformational sampling and more accurate determination of both the enthalpic and entropic contributions to the behavior of biomolecules at the Au interface in solution can be achieved (examples presented below).

## 6. Applications

As described in the previous sections, recent FF and methodological developments provide the platform for the improved and detailed understanding of the biomolecule interactions at the gold interface. This has already afforded a novel route to the generation of nanoparticle assemblies with predictable architectures<sup>[87,180]</sup> targeting specific applications. In the following sections we summarize some of the more recent studies using various computational approaches to provide molecular insight into complex bio-gold systems of relevance to several fields.

### 6.1. Nanoparticle Synthesis and Design

The design of peptide sequences that can discriminate between gold facets under aqueous conditions offer a promising route to control the growth and organization of biomimetically synthesized AuNPs. As such, computational modeling has secured an important role in emerging fields such as bionanocombinatorics and biomaterials engineering where specifically designed/encoded biomolecules and nanostructures are used to create materials and devices with unique properties and functions.

Over the years, several gold-binding peptides have been identified (summarized in reference [114]), some of which have shown binding affinities similar to those of thiols on gold. Due to the small molecular weights of these ligands,

## Experiment + Simulation

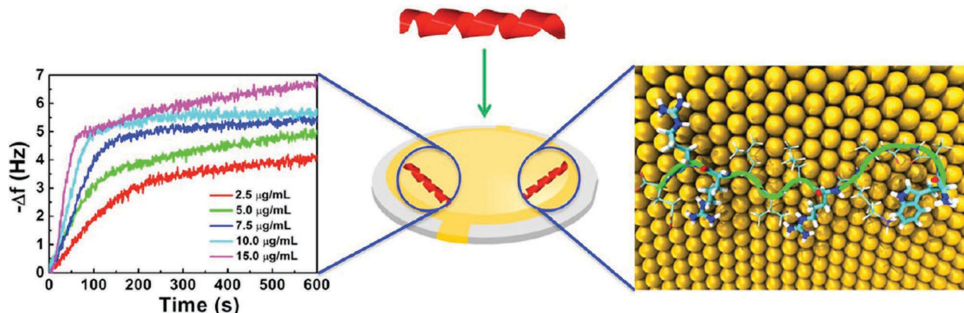


**Figure 7.** An integrated approach using experimental measurements and advanced molecular simulations was employed to establish design principles for specific interactions-driven binding sequences to gold surfaces. Reproduced with permission.<sup>[114]</sup> Copyright 2013, American Chemical Society.

they have become favorable models for molecular simulations and as such have been investigated in varying conditions using different techniques.<sup>[114a,127a,129,130,181]</sup> Initial studies describing the peptide–nanogold mechanisms of interactions focused on the enthalpic contributions to binding, by describing the probable number, distribution, and type of residue–surface contacts.<sup>[128,181a,182]</sup> Classical “brute-force” MD simulations have been also used to provide some insight into the entropic factors of binding. Vila Verde et al. explored the influence of peptide flexibility and conformational movement on peptide binding using the CHARMM22 FF and only LJ treatment for gold.<sup>[133b,181b]</sup> Heinz et al. used MD simulations and CVFF with extensions for FCC metals to estimate the configurational entropic changes of strong binding peptides adsorbing to gold.<sup>[130]</sup> Although there were some limitations in their approaches, such as the lack of structural data for comparison, the period of time over which the binding behavior was monitored and the nature of interactions with the gold surface (i.e., the surface only interacts with the peptide via dispersive interactions), their results correlated well with experimental observations. While the assumption that the gold surface does not reconstruct in response to peptide/solvent interactions is reasonable, neglecting gold surface polarization is potentially more serious. Tang et al. employed experimental methods and MD simulations using the replica exchange with solute tempering (REST) method and the polarizable GolP-CHARMM FF to study the binding of various peptide sequences to the Au(111) surface (Figure 7).<sup>[114]</sup> Their work demonstrated, quantitatively, the importance of entropically driven binding and established the design principles for creating both entropically and enthalpically driven nanomaterial-binding peptide sequences. The interplay between sequence, conformation(s) and binding propensity has a significant impact on the affinity of peptides to gold. For example, some peptide residues can show variability in their degree of surface interaction depending on their position in the chain and their immediate environment and this requires careful consideration.<sup>[183]</sup>

Several MD simulation studies have provided the structural connections between a given peptide sequence and its binding affinity to the commonly featured Au(111) and Au(100) facets,<sup>[22a,51c,118a,127a,130]</sup> which is information not easily obtained by experiment. In a recent work, Wright et al.

used the combination of REST and metadynamics simulations with the GolP-CHARMM FF to predict the adsorption free energy of a gold-binding peptide, AUBP1, at the aqueous Au(111), Au(100)(1×1) and Au(100)(5×1) interfaces.<sup>[129]</sup> Their results showed that the peptide adsorption to the Au(111) surface is stronger than to Au(100), irrespective of the reconstruction status of the latter. The surface hydration of gold was identified as the key determining factor in peptide-surface recognition, further highlighting the importance of explicit solvent treatment in classical FF simulations.

While the interactions of proteins with bare Au surfaces have been investigated in detail, albeit with differences in methodological approaches and techniques used, the study of interactions of proteins with functionalized Au surfaces is still in its infancy. In reality, bare NPs are unstable and prone to aggregation in solution. To combat this problem, NPs are often synthesized with various functional capping agents (surfactants) conjugated to their surface, such as citrates or peptide ligands, which aid the colloidal stability and solubility of the AuNPs. However, to translate this into a computational model requires an accurate description of any covalent, semi-covalent and vdW interactions between relevant gold facets and the ligated molecules. The recent development of citrate parameters for gold has enabled a more realistic representation of the functionalized gold interface in full atomic detail.<sup>[180b,184]</sup> Despite recent experimental efforts,<sup>[185]</sup> structural information about citrate anions adsorbed onto Au surfaces is still limited. From a modeling perspective, the net negative ( $-3e$ ) charge of each citrate molecule adhered to gold contributes to the electrostatic forces present at the gold interface, thus it is important to carefully consider the structure and arrangement of the adlayer. The computational studies that have looked into this differ in their treatment of the underlying gold core's surface charge. For example, Wright et al. assumed a neutral gold surface to investigate a range of citrate surface densities adsorbed at the aqueous Au(111) interface using MD simulations.<sup>[186]</sup> Their work showed that citrate overlayers are disordered, and many of their key characteristics, such as the formation of 3D rather than 2D morphologies, are invariant with surface density (Figure 8a). Generally, the anions closest to the Au surface were oriented with their carboxylate groups pointing away from the surface. The authors postulate that

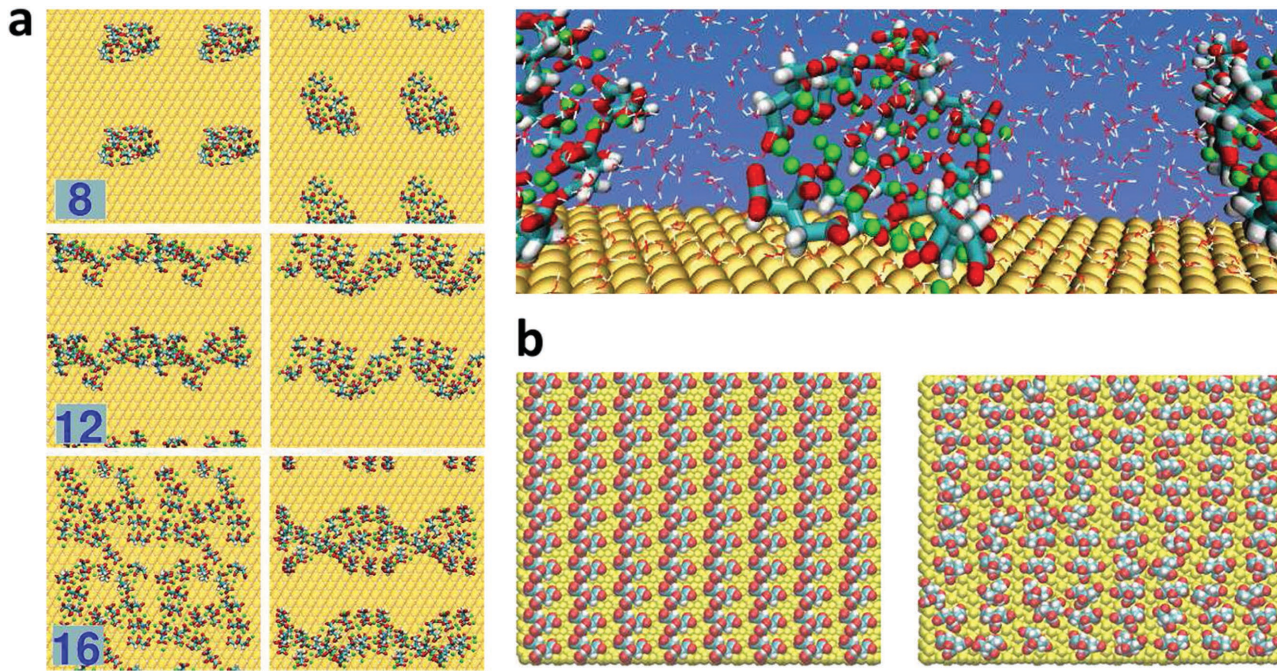


**Figure 8.** a) Citrate assemblies of varying surface densities on a neutral Au(111) surface. Adapted and reproduced with permission.<sup>[186]</sup> Copyright 2014, American Chemical Society. b) Initial (left) and final (right) citrate distribution on a positively charged Au(111) surface. Reproduced with permission.<sup>[187]</sup> Copyright 2015, American Chemical Society. These studies demonstrate the distinct structuring obtained for citrate adlayers strongly depends on the overall charge of the gold surface itself.

small biomolecules may coadsorb at the Au-citrate interface, rather than (or as well as) displace the adsorbed citrates. In contrast, Brancolini et al. studied the interaction between  $\beta_2$ -microglobulin and a citrate-coated 5 nm AuNP, using a positively charged gold core (corresponding to electrochemistry experiments).<sup>[187]</sup> Their simulations showed rigid structuring of the citrate layer without any displacement from the surface (Figure 8b). Repeating their simulations using charge neutral gold led to qualitatively similar results for the mechanisms of interactions between protein and citrate-capped gold. However, the positively charged gold core resulted in better agreement with the NMR data for  $\beta_2$ -microglobulin.

Utilizing Brancolini's approach<sup>[187]</sup> we have performed our own explicit solvent MD simulations of amylin (hIAPP) interacting with both neutral and charged citrate-coated Au(111) and Au(100) surfaces. Our simulations showed different protein behavior on the charged and neutral surfaces; however, irrespective of the gold facet and surface charge, the N-terminal region of amylin consistently displayed preferential binding to the citrate-capped gold surface.<sup>[188]</sup> This example highlights that a careful consideration of the surface and functional layer treatment in computer simulations of Au surfaces in solution is required. In a different study, the binding orientation of  $\alpha$ -synuclein to 12 nm AuNPs coated with anionic citrate and cationic (16 mercaptohexadecyl) trimethylammonium bromide (MTAB) was investigated using NMR spectroscopy and MD simulations,<sup>[189]</sup> where the interactions between the gold and the rest of the system were represented by vdW interactions only (Figure 9). Similar to our findings, their results showed that the N-terminal region of  $\alpha$ -synuclein interacted favorably with the negatively charged citrate-protected NP, while the C-terminal region was

strongly attracted to the MTAB coated NP. Despite the lack of treatment of polarization effects or crowding effects of neighboring proteins, the simulations were in agreement with the NMR results that suggested a reversal of protein binding orientation upon changing the AuNP surface charge.

MD simulations have also been able to provide insight into the mechanisms of direct electron transfer between redox proteins and electrode surfaces, which play an important role in bioelectrocatalysis, enzymatic biofuel cells and biochips.<sup>[190]</sup>

## 6.2. Targeted Applications: Biomedical Materials and Devices

Self-assembled monolayers (SAMs) impart functionality to the underlying gold nanostructures, which can be tailored to specific applications. In many cases the NP simply acts as a carrier and it is the structure and properties of the outer functional layer and/or corona formation that are of interest. Although not ideal, this may not necessarily require an explicit representation of the AuNP interactions with the environment and as such can reduce the computational cost of the simulations. Depending on the AuNP surface coverage density, and the length and type of the conjugates, the outer functional layer may be less affected by the surface due to the relatively long separations of its solvent exposed portion from the NP surface. This makes these interactions negligible and thus allows for the Au surface (and the need for specific Au surface-bio parameters) to be completely omitted from some simulation models. Several studies have employed this approach and their results were well correlated to experiments. For example, experimental protein assays and

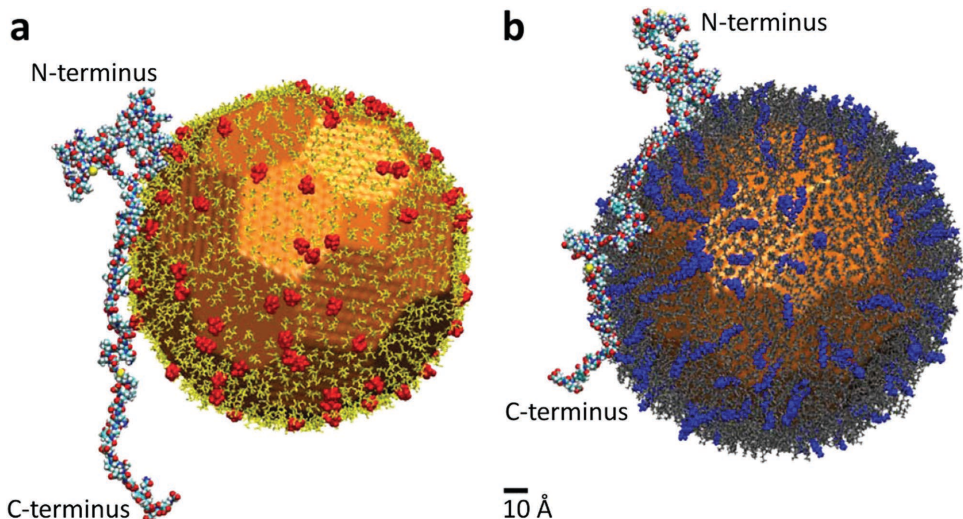


**Figure 9.** One of the largest all-atom models of protein–AuNP systems to date showing  $\alpha$ -synuclein interacting with 12 nm AuNP functionalized with a) citrate (negative) ligands, and b) MTAB (positive) conjugates. Reproduced with permission.<sup>[189]</sup> Copyright 2015, American Chemical Society.

MD simulations were used to investigate the adsorption of cytochrome C (Cyt C)<sup>[191]</sup> and lysozyme (Lyz)<sup>[192]</sup> onto monolayer-protected AuNPs where only the monolayer was represented explicitly, with regular nanoscale position variations of the hydrophobic octanethiol and hydrophilic mercaptohexanol ligands (**Figure 10a**). These simulations revealed the special role of amphipathic amino acids containing side-chain amines in facilitating direct protein adsorption to the nanostructured surfaces. Specifically, the study of Cyt C showed that lysine played a significant role in selective adsorption behavior of Cyt C on the nanostructured surfaces, while in the case of Lyz it was shown that the

amphipathic character of arginine enabled the protein to form close contacts with both polar and non-polar surface ligands simultaneously. In a separate study, using the same nanoparticles, it was shown that nanoscale structuring had an appreciable effect on the local organization, structure and energy of the interfacial solvent.<sup>[193]</sup> The authors observed non-monotonic wetting dependence on surface composition due to the formation of cavities at the liquid-solid interface and to confinement of solvent molecules over attractive domains. Overall, these findings suggested that nanopatterned surfaces can be designed with different interfacial hydrophobicity to selectively interact with different proteins,

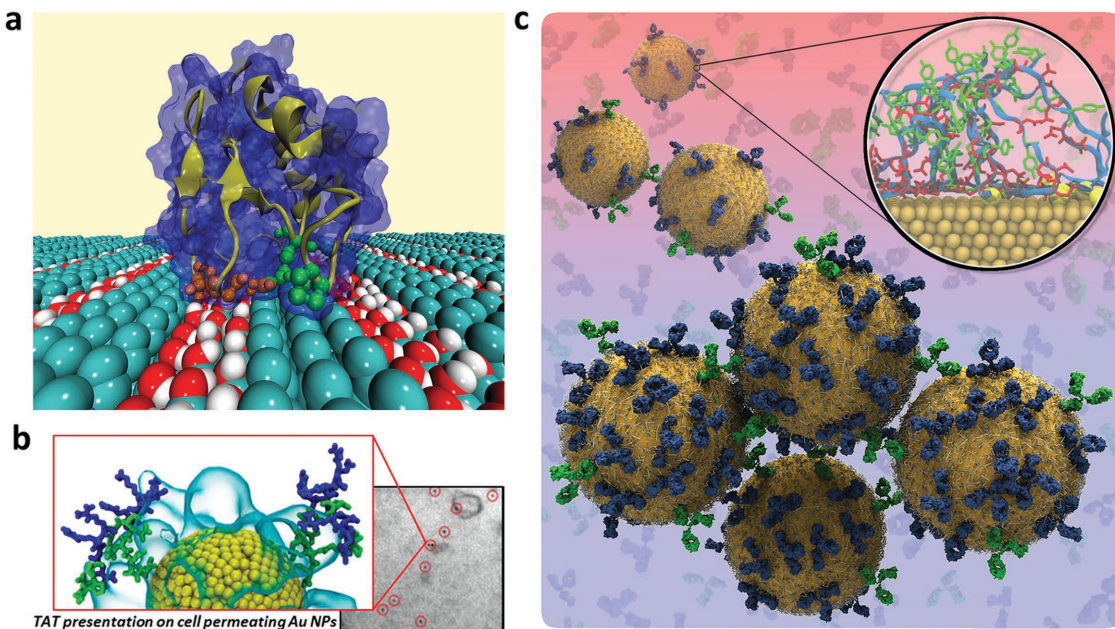


**Figure 10.** In silico studies and all-atom models of a) nanopatterned surface selectively interacting with proteins. Reproduced with permission.<sup>[192]</sup> Copyright 2013, The Royal Society of Chemistry, b) peptide functionalized nanoparticle used as cell-permeating agents. Reproduced with permission.<sup>[194]</sup> Copyright 2013, American Chemical Society and c) epitope-tagged AuNP biosensors. Adapted and reproduced with permission.<sup>[183]</sup> Copyright 2014, American Chemical Society.

and in particular amphipathic amino acids can be used to design synthetic proteins for selective adsorption on nano-patterned surfaces.

Another study where AuNPs were used as non-functional substrate carriers for functional organic layers investigated the effects of conjugate peptide concentration and distribution on small 3 nm AuNPs to aid the design of gold nanomaterials for efficient drug-delivery.<sup>[194]</sup> Nanoparticle functionalization with cell-penetrating peptides, such as the transcription transactivation TAT peptide from human HIV-1 virus, has proven to be a good strategy in the development of drug-delivery vehicles, albeit with variable performance.<sup>[195]</sup> The recent experimental and computational study reported the effects of TAT peptide concentration on the structure and dynamics of the functional layer on the 3 nm NP surface in relation to the NP's cell internalization capacity (Figure 10b).<sup>[194]</sup> Here the NP was modeled as a neutral sphere commensurate in size to 3 nm AuNP and focused on the interactions between the functional peptides and the solvent. The results provided evidence that altering concentration and distribution of the TAT peptide on the NP surface bestows distinct properties to the peptide layer structure in solution. This directly affects its membrane permeating propensity as was demonstrated by the experimental quantification of the NP cell penetration relative to TAT peptide concentration in the simulated range. This study demonstrated the need to control the structure and dynamics of functional peptides in solution in order to achieve the desired membrane-permeating activity of peptide-functionalized NPs.

On the other hand, the spontaneous fusion and membrane permeation characteristics of monolayer-protected AuNPs have been studied using simplified models.<sup>[170c,173b,196]</sup> There has also been pioneering work done by Van Lehn et al. using CG<sup>[168]</sup> and atomistic simulations,<sup>[171,196,197]</sup> where they predicted the unbiased behavior and mechanisms of interactions of ligand-functionalized NPs with cell membranes for drug-delivery and biosensing applications. Their simulations showed that the interaction with solvent-exposed lipid tail protrusions is the transition step for the insertion of AuNPs in defected and pristine bilayers. They also identified several methodological issues of importance in studying NP-bilayer interactions:<sup>[197d]</sup> (1) the careful consideration of the reaction coordinate in free energy calculations of the NP insertion process is a crucial step, while the NP-bilayer distance may be the more-widely used (and logical) reaction coordinate, considering only the distance can lead to missing the subtle interplay of lipid and ligand fluctuations identified recently;<sup>[171a,197d]</sup> (2) the necessity of free boundary conditions to accommodate the asymmetric insertion of NPs and corresponding curvature generation; and (3) the need for accurate atomistic models capable of representing the ligand flexibility and electrostatic interactions that can resolve the difference in dielectric constant between the bilayer interior and aqueous solution and corresponding free energy cost for exposing charges to a low dielectric environment.

All-atom *in silico* approaches have also been employed to provide atomistic insight into the structure and dynamics

of peptide-coated NPs to better understand the functioning of novel diagnostic sensors, and facilitate the design principles for the development of more selective and highly sensitive bioresponsive nanomaterials.<sup>[183]</sup> Recently, a single-step AuNP-based immunoassay was proposed in which the nanoparticle surface is tagged with short viral peptide epitopes (Figure 10c). Antiviral antibodies with monoclonal specificity triggered nanoparticle aggregation through a steric-kinetic mechanism, yielding a colorimetric response that enabled detection of antibodies in the low-nanomolar range within a few minutes. MD simulations using the GoLP-OPLS FF were employed to provide insights into the structural arrangement and interactions at the epitope-gold interface of different immune complexes. The results showed that the structural landscape exhibited on the surface of each epitope-gold complex was strongly influenced by peptide-peptide interactions and was thus intimately related to amino acid composition and location within individual peptide sequences.<sup>[183]</sup>

Experiments have also shown that functionalized AuNPs can be used for DNA sensing applications.<sup>[198]</sup> In particular, Mirkin and co-workers have exploited the optical properties of DNA-AuNPs to develop a highly selective colorimetric diagnostic method for DNA.<sup>[199]</sup> Additional applications may arise as a result of recent advances in the preparation of crystalline materials based on DNA-linked particles and computational insight. Even though these are challenging materials to describe due to their complexity, size, and the polyelectrolyte character of DNA, important progress has been made using all-atom and CG MD simulations, as demonstrated in a recent perspective by Lee et al.<sup>[200]</sup> For example, MD simulations have been used to characterize the conformation DNA adopts when linking AuNPs to form NP superlattice crystals.<sup>[201]</sup> Lee et al. showed that double-stranded DNA molecules transition from the A-form to B-form when connected between two Au(111) surfaces irrespective of salt-concentration or mechanical constraints imposed by the separation distance between the surfaces.<sup>[201a]</sup> Using much larger, million-atom MD simulations, Ngo et al. studied different supercrystals of DNA-functionalized 3 nm faceted AuNPs in water.<sup>[201b]</sup> Their work demonstrated noticeable differences in the linking DNA structure from that of B-form DNA due to DNA contraction, deviation in base-base stacking and hydrogen bond breaking.

### 6.3. Benign by Design: Nanotoxicology

Understanding possible adverse effects of inorganic particles on the normal structure and dynamics of biomolecules is crucial for any medical application. Nanoparticles and clusters can affect the structure of proteins and ultimately their function.<sup>[151c,202]</sup> Furthermore, due to the large surface-to-volume ratio of NPs they can promote a locally increased concentration of proteins and facilitate the formation of insoluble amyloid aggregates.<sup>[203]</sup> These amyloid fibrils are associated with many debilitating diseases<sup>[204]</sup> and recent studies suggest that depending on their size, shape and chemistry, NPs may either facilitate the formation of these toxic

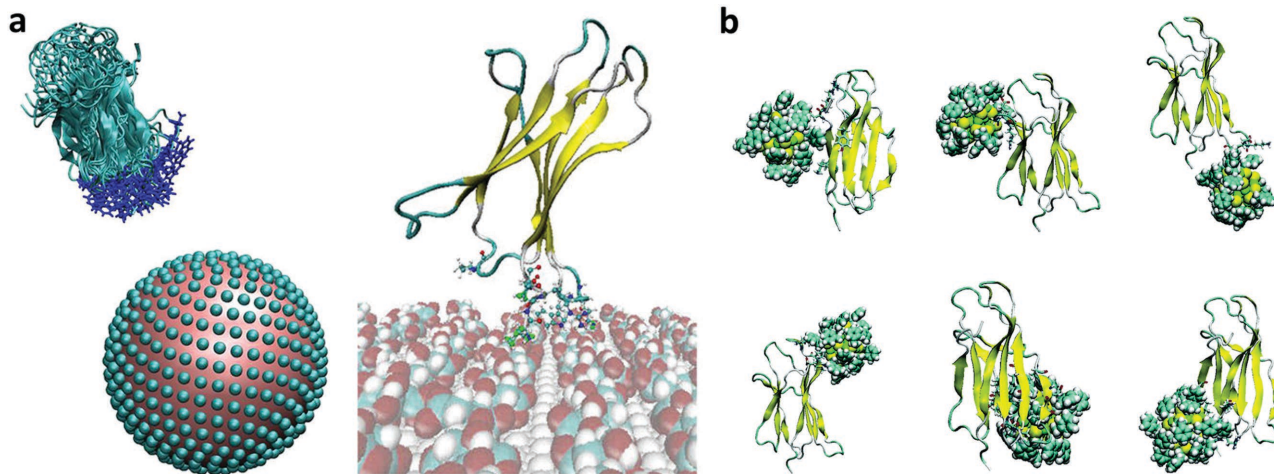


**Figure 11.** a)  $\beta_2\text{m}$  interacting with a citrate-coated nanoparticle modeled as a dielectric sphere and in all-atom detail. Reproduced with permission.<sup>[187]</sup> Copyright 2015, American Chemical Society. b)  $\beta_2\text{m}$  interacting in six favorable ways with all-atom  $\text{Au}_{25}\text{L}_{18}^-$  ( $\text{L} = \text{S}(\text{CH}_2)_2\text{Ph}$ ) AuNC. Adapted and reproduced with permission.<sup>[84b]</sup> Copyright 2014, Royal Society of Chemistry.

species<sup>[203,205]</sup> or ultimately be used as therapeutic agents for treatment of amyloid-type conditions.<sup>[6,206]</sup> In either situation, any biomedical application requires a detailed understanding of the complex interactions at the bio–nano interface. One of the initial computational studies of amyloid peptide interactions with AuNP is that by Hoefling et al. where they used GoLP-OPLS to study the adsorption mechanism of amino acids and  $\beta$ -sheet forming polypeptides on the Au(111) surface.<sup>[180c,207]</sup> Their results showed that amino acids with an intrinsic propensity to form  $\beta$ -sheets were “predisposed” to interact with gold surfaces. Their latter work showed that the adsorption of  $\beta$ -stranded peptides occurred in a step-wise mechanism on the polarized Au(111) surface, where the positively charged amino acid arginine facilitated the initial contact formation between protein and gold surface. The observation of a very fast and strong adsorption indicated that in a biological matrix, no bare gold surfaces are present, and biomolecular corona and the bioactivity of AuNPs will critically depend on the history of particle administration and the proteins present during initial contact between gold and biological material.

More recently, Brancolini et al. presented comprehensive studies based on experiment and multiple levels of theory, including docking by Brownian dynamics, Poisson–Boltzmann electrostatics calculations, and enhanced atomistic MD simulations of  $\beta_2$ -microglobulin ( $\beta_2\text{m}$ ) protein in the presence of charged (citrate-capped) AuNPs<sup>[187]</sup> and hydrophobic (thiol-protected) AuNCs (Figure 11).<sup>[84b]</sup> Their simulations showed that the interaction of  $\beta_2\text{m}$  with the charged surface of citrate-capped AuNPs did not disrupt the structure of the protein and did not form any unfolded amyloidogenic intermediates. Moreover, the MD results also suggested that the effects of protonation of certain residues, HIS31 in particular, which is known to destabilize the protein toward amyloidogenic intermediates, were enhanced by the interaction with the negative surface. Similar to their previous findings on hydrophobic AuNCs,<sup>[84b]</sup> this work highlighted that AuNP surfaces may provide either stabilizing or destabilizing effects with respect to amyloidogenic proteins and this requires a

proper balance of electrostatic and hydrophobic interactions between the NP surface and protein.

Since the ground breaking publication by Dawson et al.,<sup>[18a]</sup> it is well recognized that in the complex biological milieu, NPs adsorb a biomolecular corona which changes their physicochemical properties and confers upon them a new (and changing) bio-identity different from their properties when in pristine form. A recent experimental study showed that corona-coated AuNPs significantly reduced the amyloid inhibitory effects of the same bare NPs,<sup>[208]</sup> while other corona-coated NPs, such as graphene oxide,<sup>[209]</sup> silica, polystyrene and multi-walled carbon nanotubes,<sup>[210]</sup> showed higher inhibitory effects on amyloid- $\beta$  fibrillation compared to their respective bare particles. These studies suggest that in order to obtain a more accurate insight into the therapeutic or toxic effects of NPs, it is necessary to investigate the biological effects of the protein corona—NP complex. Mahmoudi and co-workers suggested that appropriate handling of the physicochemical properties of NPs is a promising strategy to tune the protein corona decoration, and consequently, its effect on the fibrillation process. The mechanism of protein corona formation is a complex process that depends on many parameters, such as the physicochemical properties of the NP (size, shape, composition, surface decoration, and surface charges), the nature of the physiological environment (blood, cell cytoplasm, etc.) and the duration of exposure. As a result, the temporal and spatial resolutions of all-atom simulations are unable to provide insight into all of these parameters at the same time,<sup>[211]</sup> while CG approaches can accommodate for a few parameters with reasonable computational expense, yet at the cost of atomistic detail (see Section 4 for further discussion).<sup>[181a,212]</sup> Tavanti et al. employed CG simulations to study protein corona formation on multiple citrate-coated AuNPs by two of the most abundant plasma proteins, insulin and fibrinogen (Figure 12).<sup>[167b]</sup> Their simulations included 10–100 insulin and 1–8 fibrinogen proteins in the presence of 5 nm AuNPs. Using this simplistic approach they were able to explore the protein concentration effects on NP adsorption, the competitive binding process of the two proteins on the NPs, and the dual

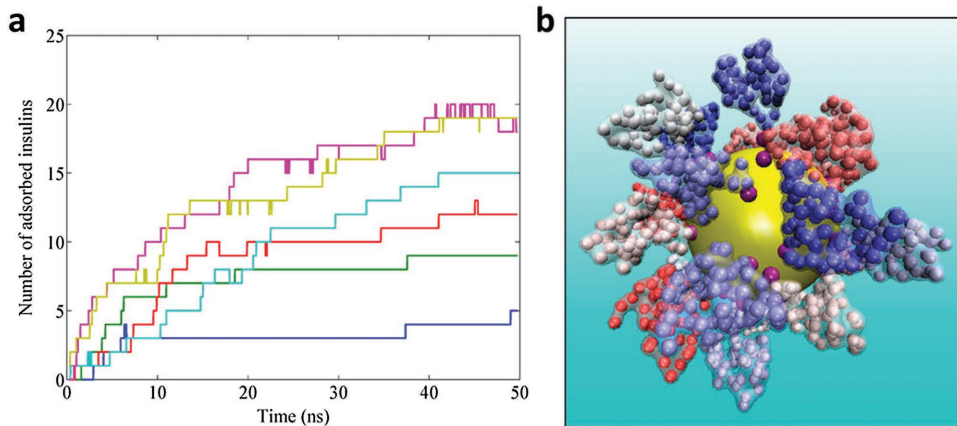


**Figure 12.** a) The number of insulin proteins bound to the citrate-coated AuNP during CG simulations at different protein concentrations: 10 (blue), 20 (green), 34 (red), 50 (cyan), 70 (purple), and 100 (brown). b) Snapshot of the protein corona formed on the citrate-coated AuNP made by 20 insulins. Reproduced with permission.<sup>[167b]</sup> Copyright 2015, American Chemical Society.

NP binding to fibrinogen in comparison with experiment. In a similar work, CG simulations were used to study ubiquitin corona formation on AuNPs of different sizes (10, 16, 20 and 24 nm diameters) in bare and citrate-coated forms.<sup>[167a]</sup>

It is evident that advances in simulation algorithms and “petascale” computing capabilities are moving the atomic resolution models of biological systems into the million-to-billion atom regime, providing insight in the structure and real time evolution of supramolecular complexes. A recent review highlights the progress driven by large-scale MD simulations in applications ranging from cell biology to health sciences to biofuel production,<sup>[213]</sup> re-emphasizing the ever-increasing role of simulations as a ‘computational microscope’<sup>[214]</sup> complementary to experiments. These and other examples highlight the ability of theoretical simulations to help derive the understanding necessary for designing Au nanomaterials for precise targeting in biological medium while avoiding undesirable non-specific adsorption processes. The growth in successful applications of computational studies in conjunction with experiments will enable the “benign by design” concept for nanomedicine to be a reality sooner rather than later.

## 7. Conclusions and Perspectives

This article provides an overview on the current computational developments (advances and challenges) with examples of recent applications of Au–bio interfacial systems.

A consensus seems to have been reached in the computational community, evident throughout this review, that no single molecular modeling approach, from electronic structure calculations (primarily DFT based), classical all-atom MD through to CG MD, is currently capable of describing the AuNP–bio interface in all its complexity. Therefore, a so-called multiscale approach has emerged as a way to describe and model these systems in the quest for a comprehensive physicochemical description of the phenomena involved. One can define multiscale modeling as an approach involving at least one of the following combinations used for a system of interest:

1. One level of model representation enables another, e.g., electronic structure methods used to develop classical FF for a particular system; classical FF methods used to get binding free energies that are used to develop a CG FF.
2. At least two approximation levels are used to model the same system to get physicochemical effects at different time and length scales, e.g., classical methods used to obtain an equilibrium geometry for a nano–bio interface in solution, followed by an electronic structure calculation of the equilibrated system to obtain the electron density redistribution at the interface.
3. A multiscale treatment of the complete system, where the region of interest is modeled at high resolution and the surrounding environment at a lower level of resolution. An example of this is the QM/MM methodology, where there is a static division between the two resolution methods, or the AdResS (Adaptive Resolution Simulation) scheme,<sup>[215]</sup> which combines the advantages of all-atom and CG models and allows particles to change resolution on-the-fly. For each of these methods, however, applications have so far been limited to simple test systems. The real benefit of such multiscale methods has yet to come.

In relation to AuNPs specifically, the fluorescent and plasmonic properties, as well as the thiol functionalization chemistry employed for the majority of engineered AuNPs inherently involve electronic effects. On the other hand, the packing of ligands on NP surfaces as well as the conformational responses of proteins and lipid bilayers to the presence of AuNPs are largely governed by physical interactions (due to electrostatic and vdW forces). Polarizability of Au substrates, solvents (water, salts, etc.), and variations in pH affect both electronic and conformational properties and, in principle, must be considered at both levels. Coarse-graining becomes useful when the packing and self-assembly of ligands, or the AuNPs themselves, become the point of main interest, yet it loses chemical detail and the interaction potentials in these methods must ultimately rely on finer all-atom and electronic structure methods. Similarly, the ongoing refinement of all-atom FFs is likely to rely on electronic structure calculations for years ahead and ultimately

a “globalization” (generalization) of FFs will enable one to reliably treat any combination of molecular components within a single interaction potential framework. This remains a highly desirable but an extremely challenging outcome. For the time being, it is crucial we have accurate and consistent FFs allowing the description of real inorganic systems whose complexity may be related to the variety of interactions sites including faces, edges, vertices and/or the presence of surfactants covering the surface and altering the interaction with water and other biomolecules.

The ultimate power of electronic structure methods to treat any system in principle, in reality is limited not only by computational capacity but also by the range of approximations currently involved in the methodologies themselves, e.g., representation of the electron density and electron correlation effects for complex systems, such as nano–bio interfaces in solvent. While linear-scaling DFT methods show the most promise, they still need significant developments to become a routine tool for modeling the dynamic evolution of biologically relevant nano–bio systems. Yet these methods are indispensable for: understanding electron transfer and polarization effects at nano–bio interfaces, which remain generally out of reach for classical MD; and to get the classical FFs right.

Clearly, enhanced sampling techniques will remain topical at least until computational power enables the spontaneous evolution of systems to be monitored for biologically relevant time scales. Even then, the motivation from the experimental perspective to continuously increase the size and comprehensiveness of molecular models will likely bring the level of computational resources back to deficient despite Moore’s Law, in a cyclical manner.

Importantly, idealized models lacking experimental (let alone living tissue) complexity will remain the biggest challenge for both the experimental and theoretical communities to overcome in order to achieve direct transferability between modeling and experimental results, and a straightforward translation to treatment of disease or medical diagnostic technologies.

Despite all current approximations, limitations, and remaining challenges, multiscale molecular modeling has been able to provide non-intuitive insights in the nano–bio interface structure and properties at the electronic and all-atom levels that were not achievable through any other techniques, and will therefore remain an indispensable tool for obtaining fundamental knowledge of gold (and other) nano–bio systems, enabling major technological breakthroughs in medicine and other fields of human endeavor.

## Acknowledgments

The authors would like to thank A/Prof. Nicholas D. M. Hine (The University of Warwick) for useful discussions. I.Y. acknowledges the Australian Research Council for financial support under the Discovery Project scheme (DP140101888).

- [1] a) P. D. Howes, R. Chandrawati, M. M. Stevens, *Science* **2014**, *346*, 1247390; b) K. Saha, S. S. Agasti, C. Kim, X. Li, V. M. Rotello, *Chem. Rev.* **2012**, *112*, 2739.
- [2] a) M. Cui, Y. Zhao, Q. Song, *Trend. Anal. Chem.* **2014**, *57*, 73; b) V. K. A. Sreenivasan, A. V. Zvyagin, E. M. Goldys, *J. Phys.: Condens. Matter* **2013**, *25*, 194101; c) L.-Y. Chen, C.-W. Wang, Z. Yuan, H.-T. Chang, *Anal. Chem.* **2015**, *87*, 216.
- [3] G. Ajnai, A. Chiu, T. Kan, C.-C. Cheng, T.-H. Tsai, J. Chang, *J. Exp. Clin. Med.* **2014**, *6*, 172.
- [4] M. Yamada, M. Foote, T. W. Prow, *Wiley Interdiscip. Rev.: Nanomed. Nanobiotechnol.* **2015**, *7*, 428.
- [5] Y. Zhang, T. P. Shareena Dasari, H. Deng, H. Yu, *J. Environ. Sci. Health Part C: Environ. Carcinog. Ecotoxicol. Rev.* **2015**, *33*, 286.
- [6] E.-K. Lim, T. Kim, S. Paik, S. Haam, Y.-M. Huh, K. Lee, *Chem. Rev.* **2015**, *115*, 327.
- [7] N. Goswami, K. Zheng, J. Xie, *Nanoscale* **2014**, *6*, 13328.
- [8] W. Sun, A. Ferretti, D. Varsano, G. Brancolini, S. Corni, R. Di Felice, *J. Phys. Chem. C* **2014**, *118*, 18820.
- [9] T. M. Carducci, R. E. Blackwell, R. W. Murray, *J. Phys. Chem. Lett.* **2015**, *6*, 1299.
- [10] a) C. Vericat, M. E. Vela, G. Benitez, P. Carro, R. C. Salvarezza, *Chem. Soc. Rev.* **2010**, *39*, 1805; b) F. Hanke, J. Björk, *Phys. Rev. B* **2013**, *87*, 235422.
- [11] L. Shang, Y. Wang, J. Jiang, S. Dong, *Langmuir* **2007**, *23*, 2714.
- [12] H. Heinz, T.-J. Lin, R. Kishore Mishra, F. S. Emami, *Langmuir* **2013**, *29*, 1754.
- [13] A. Leifert, Y. Pan-Bartnek, U. Simon, W. Jahnens-Dechent, *Nanoscale* **2013**, *5*, 6224.
- [14] W. Humphrey, A. Dalke, K. Schulter, *J. Mol. Graph.* **1996**, *14*, 33.
- [15] J. J. Wiltzius, S. A. Sievers, M. R. Sawaya, D. Cascio, D. Popov, C. Riekel, D. Eisenberg, *Protein Sci.* **2008**, *17*, 1467.
- [16] a) C. L. Heinecke, T. W. Ni, S. Malola, V. Mäkinen, O. A. Wong, H. Häkkinen, C. J. Ackerson, *J. Am. Chem. Soc.* **2012**, *134*, 13316; b) M. W. Heaven, A. Dass, P. S. White, K. M. Holt, R. W. Murray, *J. Am. Chem. Soc.* **2008**, *130*, 3754.
- [17] a) T. L. Moore, L. Rodriguez-Lorenzo, V. Hirsch, S. Balog, D. Urban, C. Jud, B. Rothen-Rutishauser, M. Lattuada, A. Petri-Fink, *Chem. Soc. Rev.* **2015**; b) D. Docter, D. Westmeier, M. Markiewicz, S. Stolte, S. K. Knauer, R. H. Stauber, *Chem. Soc. Rev.* **2015**, *44*, 6094; c) C. M. Beddoes, C. P. Case, W. H. Briscoe, *Adv. Colloid Interface Sci.* **2015**, *218*, 48; d) S.-T. Yang, Y. Liu, Y.-W. Wang, A. Cao, *Small* **2013**, *9*, 1635; e) J. Zheng, C. Zhou, M. Yu, J. Liu, *Nanoscale* **2012**, *4*, 4073.
- [18] a) M. P. Monopoli, C. Aberg, A. Salvati, K. A. Dawson, *Nat. Nanotechnol.* **2012**, *7*, 779; b) C. Ge, J. Tian, Y. Zhao, C. Chen, R. Zhou, Z. Chai, *Arch. Toxicol.* **2015**, *89*, 519.
- [19] J. A. Pople, *Angew. Chem. Int. Ed.* **1999**, *38*, 1894.
- [20] F. De Proft, P. Geerlings, *Chem. Rev.* **2001**, *101*, 1451.
- [21] A. R. Leach, *Molecular Modeling: Principles and Applications*, 2nd ed., Prentice Hall, Harlow, Essex, UK **2001**.
- [22] a) J. Yu, M. L. Becker, G. A. Carri, *Small* **2010**, *6*, 2242; b) W. Kurashige, Y. Niihori, S. Sharma, Y. Negishi, *J. Phys. Chem. Lett.* **2014**, *5*, 4134; c) H. Häkkinen, *Nat. Chem.* **2012**, *4*, 443; d) D.-e. Jiang, *Nanoscale* **2013**, *5*, 7149.
- [23] M. Azubel, J. Koivisto, S. Malola, D. Bushnell, G. L. Hura, A. L. Koh, H. Tsunoyama, T. Tsukuda, M. Pettersson, H. Häkkinen, R. D. Kornberg, *Science* **2014**, *345*, 909.
- [24] J. Akola, M. Walter, R. L. Whetten, H. Häkkinen, H. Grönbeck, *J. Am. Chem. Soc.* **2008**, *130*, 3756.
- [25] M. Zhu, C. M. Aikens, F. J. Hollander, G. C. Schatz, R. Jin, *J. Am. Chem. Soc.* **2008**, *130*, 5883.
- [26] O. Lopez-Acevedo, H. Tsunoyama, T. Tsukuda, H. Häkkinen, C. M. Aikens, *J. Am. Chem. Soc.* **2010**, *132*, 8210.
- [27] H. Qian, W. T. Eckenhoff, Y. Zhu, T. Pintauer, R. Jin, *J. Am. Chem. Soc.* **2010**, *132*, 8280.
- [28] a) Y. Pei, J. Tang, X. Tang, Y. Huang, X. C. Zeng, *J. Phys. Chem. Lett.* **2015**, *6*, 1390; b) Y. Yu, Z. Luo, D. M. Chevrier, D. T. Leong,

- P. Zhang, D.-e. Jiang, J. Xie, *J. Am. Chem. Soc.* **2014**, *136*, 1246.
- [29] P. R. Nimmala, B. Yoon, R. L. Whetten, U. Landman, A. Dass, *J. Phys. Chem. A* **2013**, *117*, 504.
- [30] D. Bahena, N. Bhattacharai, U. Santiago, A. Tlahuice, A. Ponce, S. B. H. Bach, B. Yoon, R. L. Whetten, U. Landman, M. Jose-Yacaman, *J. Phys. Chem. Lett.* **2013**, *4*, 975.
- [31] D. F. Yancey, S. T. Chill, L. Zhang, A. I. Frenkel, G. Henkelman, R. M. Crooks, *Chem. Sci.* **2013**, *4*, 2912.
- [32] A. Tlahuice-Flores, *Phys. Chem. Chem. Phys.* **2015**, *17*, 5551.
- [33] H. Qian, Y. Zhu, R. Jin, *Proc. Natl. Acad. Sci. USA* **2012**, *109*, 696.
- [34] A. Cossaro, R. Mazzarello, R. Rousseau, L. Casalis, A. Verdini, A. Kohlmeyer, L. Floreano, S. Scandolo, A. Morgante, M. L. Klein, G. Scoles, *Science* **2008**, *321*, 943.
- [35] M. Walter, J. Akola, O. Lopez-Acevedo, P. D. Jazdinsky, G. Calero, C. J. Ackerson, R. L. Whetten, H. Grönbeck, H. Häkkinen, *Proc. Natl. Acad. Sci. USA* **2008**, *105*, 9157.
- [36] Y. Negishi, N. K. Chaki, Y. Shichibu, R. L. Whetten, T. Tsukuda, *J. Am. Chem. Soc.* **2007**, *129*, 11322.
- [37] Y. Negishi, T. Nakazaki, S. Malola, S. Takano, Y. Niihori, W. Kurashige, S. Yamazoe, T. Tsukuda, H. Häkkinen, *J. Am. Chem. Soc.* **2015**, *137*, 1206.
- [38] L. Sementa, G. Barcaro, A. Dass, M. Stener, A. Fortunelli, *Chem. Commun.* **2015**, *51*, 7935.
- [39] J. Zhong, X. Tang, J. Tang, J. Su, Y. Pei, *J. Phys. Chem. C* **2015**, *119*, 9205.
- [40] F. Muniz-Miranda, M. C. Menziani, A. Pedone, *J. Phys. Chem. C* **2014**, *118*, 7532.
- [41] M. Couty, M. B. Hall, *J. Comput. Chem.* **1996**, *17*, 1359.
- [42] a) A. Castro, M. A. L. Marques, A. H. Romero, M. J. T. Oliveira, A. Rubio, *J. Chem. Phys.* **2008**, *129*, 144110; b) H. Häkkinen, M. Moseler, U. Landman, *Phys. Rev. Lett.* **2002**, *89*, 033401.
- [43] J. Autschbach, *J. Chem. Phys.* **2012**, *136*, 150902.
- [44] Y. Pei, R. Pal, C. Liu, Y. Gao, Z. Zhang, X. C. Zeng, *J. Am. Chem. Soc.* **2012**, *134*, 3015.
- [45] A. Das, T. Li, G. Li, K. Nobusada, C. Zeng, N. L. Rosi, R. Jin, *Nanoscale* **2014**, *6*, 6458.
- [46] a) R. Ouyang, Y. Xie, D.-e. Jiang, *Nanoscale* **2015**, *7*, 14817; b) L. A. Mancera, D. M. Benoit, *Comput. Theor. Chem.* **2015**, *1067*, 24.
- [47] A. Bruma, R. Ismail, L. Oliver Paz-Borbon, H. Arslan, G. Barcaro, A. Fortunelli, Z. Y. Li, R. L. Johnston, *Nanoscale* **2013**, *5*, 646.
- [48] a) Z. Wu, J. Liu, Y. Li, Z. Cheng, T. Li, H. Zhang, Z. Lu, B. Yang, *ACS Nano* **2015**, *9*, 6315; b) X.-N. Zhang, R. Wang, G. Xue, *Chin. Phys. B* **2014**, *23*, 098201; c) S. M. Neidhart, B. M. Barnsgrover, C. M. Aikens, *Phys. Chem. Chem. Phys.* **2015**, *17*, 7676.
- [49] a) K.-M. Xu, T. Huang, H. Wen, Y.-R. Liu, Y.-B. Gai, W.-J. Zhang, W. Huang, *RSC Adv.* **2013**, *3*, 24492; b) H. Yang, Y. Wang, J. Lei, L. Shi, X. Wu, V. Mäkinen, S. Lin, Z. Tang, J. He, H. Häkkinen, L. Zheng, N. Zheng, *J. Am. Chem. Soc.* **2013**, *135*, 9568; c) V. G. Yarzhemsky, M. A. Kazaryan, N. A. Bulychev, E. N. Muraviev, Y. A. Dyakov, O. K. Kosheleva, C. H. Chen, *J. Nanotechnol. Diagn. Treat.* **2014**, *2*, 27.
- [50] A. Trinchero, S. Klacar, L. O. Paz-Borbón, A. Hellman, H. Grönbeck, *J. Phys. Chem. C* **2015**, *119*, 10797.
- [51] a) A. Hadley, C. M. Aikens, *J. Phys. Chem. C* **2010**, *114*, 18134; b) A. Fernando, C. M. Aikens, *J. Phys. Chem. C* **2015**, *119*, 20179; c) J. Jung, S. Kang, Y.-K. Han, *Nanoscale* **2012**, *4*, 4206; d) N. Takagi, K. Ishimura, M. Matsui, R. Fukuda, T. Matsui, T. Nakajima, M. Ehara, S. Sakaki, *J. Am. Chem. Soc.* **2015**, *137*, 8593.
- [52] a) E. Fertitta, E. Voloshina, B. Paulus, *J. Comput. Chem.* **2014**, *35*, 204; b) D. Mollenhauer, N. Gaston, E. Voloshina, B. Paulus, *J. Phys. Chem. C* **2013**, *117*, 4470; c) R. Ouyang, J. Yan, P. S. Jensen, E. Ascic, S. Gan, D. Tanner, B. Mao, L. Niu, J. Zhang, C. Tang, N. S. Hush, J. R. Reimers, J. Ulstrup, *ChemPhysChem* **2015**, *16*, 928.
- [53] a) H. Barron, L. Fernández-Seivane, X. López-Lozano, *Phys. Status Solidi B* **2014**, *251*, 1239; b) F. Dufour, B. Fresch, O. Durupthy, C. Chaneac, F. Remacle, *J. Phys. Chem. C* **2014**, *118*, 4362; c) X.-J. Liu, I. Hamilton, *J. Comput. Chem.* **2014**, *35*, 1967.
- [54] A. S. Barnard, *Cryst. Growth Des.* **2013**, *13*, 5433.
- [55] a) B. M. Barnsgrover, C. M. Aikens, *J. Phys. Chem. A* **2013**, *117*, 5377; b) V. Rojas-Cervellera, E. Giralt, C. Rovira, *Inorg. Chem.* **2012**, *51*, 11422.
- [56] M. Askerka, D. Pichugina, N. Kuz'menko, A. Shestakov, *J. Phys. Chem. A* **2012**, *116*, 7686.
- [57] a) J. R. Reimers, Y. Wang, B. O. Cankurtaran, M. J. Ford, *J. Am. Chem. Soc.* **2010**, *132*, 8378; b) J. Yan, R. Ouyang, P. S. Jensen, E. Ascic, D. Tanner, B. Mao, J. Zhang, C. Tang, N. S. Hush, J. Ulstrup, J. R. Reimers, *J. Am. Chem. Soc.* **2014**, *136*, 17087.
- [58] S. Sharma, W. Kurashige, K. Nobusada, Y. Negishi, *Nanoscale* **2015**, *7*, 10606.
- [59] I. Dolamic, B. Varnholt, T. Bürgi, *Nat. Commun.* **2015**, *6*, 7117.
- [60] K. Forster-Tonigold, A. Groß, *Surf. Sci.* **2015**, *640*, 18.
- [61] A. Mathew, G. Natarajan, L. Lehtovaara, H. Häkkinen, R. M. Kumar, V. Subramanian, A. Jaleel, T. Pradeep, *ACS Nano* **2014**, *8*, 139.
- [62] a) J. Polte, *CrystEngComm* **2015**, *17*, 6809; b) C. Liu, Y. Pei, H. Sun, J. Ma, *J. Am. Chem. Soc.* **2015**, *137*, 15809.
- [63] C. Adamo, D. Jacquemin, *Chem. Soc. Rev.* **2013**, *42*, 845.
- [64] P. N. Day, K. A. Nguyen, R. Pachter, *J. Chem. Theory Comput.* **2010**, *6*, 2809.
- [65] S. Antonello, N. V. Perera, M. Ruzzi, J. A. Gascón, F. Maran, *J. Am. Chem. Soc.* **2013**, *135*, 15585.
- [66] A. Tlahuice-Flores, R. L. Whetten, M. Jose-Yacaman, *J. Phys. Chem. C* **2013**, *117*, 20867.
- [67] a) S. Chen, S. Wang, J. Zhong, Y. Song, J. Zhang, H. Sheng, Y. Pei, M. Zhu, *Angew. Chem. Int. Ed.* **2015**, *54*, 3145; b) A. Das, C. Liu, H. Y. Byun, K. Nobusada, S. Zhao, N. Rosi, R. Jin, *Angew. Chem. Int. Ed.* **2015**, *54*, 3140.
- [68] A. Fihey, F. Maurel, A. Perrier, *J. Phys. Chem. C* **2014**, *118*, 4444.
- [69] A. Fihey, F. Maurel, A. Perrier, *Phys. Chem. Chem. Phys.* **2014**, *16*, 26240.
- [70] a) A. Fihey, B. Le Guennic, D. Jacquemin, *J. Phys. Chem. Lett.* **2015**, *6*, 3067; b) A. Fihey, F. Maurel, A. Perrier, *J. Phys. Chem. C* **2015**, *119*, 9995.
- [71] H. C. Weissker, O. Lopez-Acevedo, R. L. Whetten, X. López-Lozano, *J. Phys. Chem. C* **2015**, *119*, 11250.
- [72] a) E. B. Guidez, C. M. Aikens, *J. Phys. Chem. A* **2015**, *119*, 3337; b) Q. Meng, S. P. May, M. T. Berry, D. S. Kilin, *Mol. Phys.* **2015**, *113*, 408; c) X. López Lozano, C. Mottet, H. C. Weissker, *J. Phys. Chem. C* **2013**, *117*, 3062.
- [73] F. Muniz-Miranda, M. C. Menziani, A. Pedone, *J. Phys. Chem. C* **2015**, *119*, 10766.
- [74] E. Pohjolainen, H. Häkkinen, A. Clayborne, *J. Phys. Chem. C* **2015**, *119*, 9587.
- [75] G. Lugo, V. Schwanen, B. Fresch, F. Remacle, *J. Phys. Chem. C* **2015**, *119*, 10969.
- [76] A. Tlahuice-Flores, R. L. Whetten, M. Jose-Yacaman, *J. Phys. Chem. C* **2013**, *117*, 12191.
- [77] A. Angioni, S. Corni, B. Mennucci, *Phys. Chem. Chem. Phys.* **2013**, *15*, 3294.
- [78] X.-K. Wan, W. W. Xu, S.-F. Yuan, Y. Gao, X.-C. Zeng, Q.-M. Wang, *Angew. Chem. Int. Ed.* **2015**, *54*, 9683.
- [79] K. Moth-Poulsen, *Handbook of Single-Molecule Electronics*, Pan Stanford, Singapore **2015**.
- [80] a) J. Klimeš, A. Michaelides, *J. Chem. Phys.* **2012**, *137*, 120901; b) P. Tereshchuk, J. L. F. Da Silva, *J. Phys. Chem. C* **2012**, *116*, 24695; c) W. Liu, J. Carrasco, B. Santra, A. Michaelides, M. Scheffler, A. Tkatchenko, *Phys. Rev. B* **2012**, *86*, 245405; d) T. S. Chwee, M. B. Sullivan, *J. Chem. Phys.* **2012**, *137*, 134703;

- e) J. L. C. Fajín, F. Teixeira, J. R. B. Gomes, M. N. D. S. Cordeiro, *Theor. Chem. Acc.* **2015**, *134*, 67.
- [81] a) R. Nadler, J. F. Sanz, *J. Chem. Phys.* **2012**, *137*, 114709; b) J. Carrasco, J. Klimeš, A. Michaelides, *J. Chem. Phys.* **2013**, *138*, 024708; c) K. Tonigold, A. Groß, *J. Comput. Chem.* **2012**, *33*, 695.
- [82] L. B. Wright, P. M. Rodger, S. Corni, T. R. Walsh, *J. Chem. Theory Comput.* **2013**, *9*, 1616.
- [83] a) S. Piana, A. Bilic, *J. Phys. Chem. B* **2006**, *110*, 23467; b) F. Iori, R. Di Felice, E. Molinari, S. Corni, *J. Comput. Chem.* **2009**, *30*, 1465.
- [84] a) S. Banerjee, J. A. Montgomery Jr., J. A. Gascón, *J. Mater. Sci.* **2012**, *47*, 7686; b) G. Brancolini, D. Toroz, S. Corni, *Nanoscale* **2014**, *6*, 7903.
- [85] a) M. Dion, H. Rydberg, E. Schröder, D. C. Langreth, B. I. Lundqvist, *Phys. Rev. Lett.* **2004**, *92*, 246401; b) T. Thonhauser, V. R. Cooper, S. Li, A. Puzder, P. Hyldgaard, D. C. Langreth, *Phys. Rev. B* **2007**, *76*, 125112.
- [86] B. Hammer, L. B. Hansen, J. K. Nørskov, *Phys. Rev. B* **1999**, *59*, 7413.
- [87] M. Hoefling, F. Iori, S. Corni, K.-E. Gottschalk, *ChemPhysChem* **2010**, *11*, 1763.
- [88] G. Hong, H. Heinz, R. R. Naik, B. L. Farmer, R. Pachter, *ACS Appl. Mater. Interfaces* **2009**, *1*, 388.
- [89] Y. Zhao, F. Zhou, H. Zhou, H. Su, *Phys. Chem. Chem. Phys.* **2013**, *15*, 1690.
- [90] H.-J. Xie, Q.-F. Lei, W.-J. Fang, *J. Mol. Model.* **2012**, *18*, 645.
- [91] A. H. Pakiari, Z. Jamshidi, *J. Phys. Chem. A* **2007**, *111*, 4391.
- [92] Z. Aliakbar Tehrani, Z. Jamshidi, M. Jebeli Javan, A. Fattahi, *J. Phys. Chem. A* **2012**, *116*, 4338.
- [93] V. Rojas-Cervellera, C. Rovira, J. Akola, *J. Phys. Chem. Lett.* **2015**, 3859.
- [94] L. Zhang, T. Ren, X. Yang, L. Zhou, X. Li, *Int. J. Quantum Chem.* **2013**, *113*, 2234.
- [95] A. Sarmah, R. K. Roy, *J. Phys. Chem. C* **2015**, *119*, 17940.
- [96] S. Rai, H. Singh, U. D. Priyakumar, *RSC Adv.* **2015**, *5*, 49408.
- [97] A. Dass, S. Theivendran, P. R. Nimmala, C. Kumara, V. R. Jupally, A. Fortunelli, L. Sementa, G. Barcaro, X. Zuo, B. C. Noll, *J. Am. Chem. Soc.* **2015**, *137*, 4610.
- [98] a) P. Koskinen, V. Mäkinen, *Comput. Mater. Sci.* **2009**, *47*, 237; b) V. Mäkinen, P. Koskinen, H. Häkkinen, *Eur. Phys. J. D* **2013**, *67*, 38; c) L. Rincon, A. Hasmy, M. Marquez, C. Gonzalez, *Chem. Phys. Lett.* **2011**, *503*, 171; d) P. Koskinen, H. Häkkinen, G. Seifert, S. Sanna, T. Frauenheim, M. Moseler, *New J. Phys.* **2006**, *8*, 9.
- [99] a) J. J. Stewart, *J. Mol. Model.* **2007**, *13*, 1173; b) W. Thiel, *Wiley Interdiscip. Rev.: Comput. Mol. Sci.* **2014**, *4*, 145.
- [100] a) C. K. Skylaris, P. D. Haynes, A. A. Mostofi, M. C. Payne, *J. Phys.: Condens. Matter* **2005**, *17*, 5757; b) A. A. Mostofi, P. D. Haynes, C. K. Skylaris, M. C. Payne, *Mol. Simul.* **2007**, *33*, 551.
- [101] J. M. Soler, E. Artacho, J. D. Gale, A. Garcia, J. Junquera, P. Ordejón, D. Sánchez-Portal, *J. Phys.: Condens. Matter* **2002**, *14*, 2745.
- [102] A. Ruiz-Serrano, C. K. Skylaris, *J. Chem. Phys.* **2013**, *139*, 054107.
- [103] L. Lee, P. D. Cole, J. M. Payne, C. C.-K. Skylaris, *J. Comput. Chem.* **2013**, *34*, 429.
- [104] N. Todorova, A. J. Makarucha, N. D. M. Hine, A. A. Mostofi, I. Yarovsky, *PLoS Comput. Biol.* **2013**, *9*, e1003360.
- [105] H. C. Wang, Y. S. Leng, *J. Phys. Chem. C* **2015**, *119*, 15216.
- [106] C. R. L. Chapman, E. C. M. Ting, A. Kereszti, I. Paci, *J. Phys. Chem. C* **2013**, *117*, 19426.
- [107] M. L. Sushko, P. V. Sushko, I. V. Abarenkov, A. L. Shluger, *J. Comput. Chem.* **2010**, *31*, 2955.
- [108] J. Schneider, L. Colombi Ciacchi, *J. Am. Chem. Soc.* **2012**, *134*, 2407.
- [109] W. D. Cornell, P. Cieplak, C. I. Bayly, I. R. Gould, K. M. Merz, D. M. Ferguson, D. C. Spellmeyer, T. Fox, J. W. Caldwell, P. A. Kollman, *J. Am. Chem. Soc.* **1995**, *117*, 5179.
- [110] A. D. MacKerell, D. Bashford, M. Bellott, R. L. Dunbrack, J. D. Evanseck, M. J. Field, S. Fischer, J. Gao, H. Guo, S. Ha, D. Joseph-McCarthy, L. Kuchnir, K. Kuczera, F. T. K. Lau, C. Mattos, S. Michnick, T. Ngo, D. T. Nguyen, B. Prodhom, W. E. Reiher III, B. Roux, M. Schlenkrich, J. C. Smith, R. Stote, J. Straub, M. Watanabe, J. Wiorkiewicz-Kuczera, D. Yin, M. Karplus, *J. Phys. Chem. B* **1998**, *102*, 3586.
- [111] L. D. Schuler, X. Daura, W. F. van Gunsteren, *J. Comput. Chem.* **2001**, *22*, 1205.
- [112] W. L. Jorgensen, D. S. Maxwell, J. Tirado-Rives, *J. Am. Chem. Soc.* **1996**, *118*, 11225.
- [113] R. A. Latour, *Colloids Surf. B* **2014**, *124*, 25.
- [114] Z. Tang, J. P. Palafox-Hernandez, W.-C. Law, Z. E. Hughes, M. T. Swihart, P. N. Prasad, M. R. Knecht, T. R. Walsh, *ACS Nano* **2013**, *7*, 9632.
- [115] G. Heimel, J.-L. Brédas, *Nat. Nanotechnol.* **2013**, *8*, 230.
- [116] F. Iori, S. Corni, *J. Comput. Chem.* **2008**, *29*, 1656.
- [117] a) X. Chen, O. V. Prezhdo, Z. Ma, T. Hou, Z. Guo, Y. Li, *Phys. Status Solidi B* **2015**; b) L. L. Jensen, L. Jensen, *J. Phys. Chem. C* **2008**, *112*, 15697.
- [118] H. Heinz, K. C. Jha, J. Luettmer-Strathmann, B. L. Farmer, R. R. Naik, *J. R. Soc. Interface* **2011**, *8*, 220.
- [119] K. C. Jha, H. Liu, M. R. Bockstaller, H. Heinz, *J. Phys. Chem. C* **2013**, *117*, 25969.
- [120] H. Heinz, H. Ramezani-Dakhel, *Chem. Soc. Rev.* **2016**, *45*, 412.
- [121] L. B. Wright, P. M. Rodger, T. R. Walsh, S. Corni, *J. Phys. Chem. C* **2013**, *117*, 24292.
- [122] H. Heinz, R. A. Vaia, B. L. Farmer, R. R. Naik, *J. Phys. Chem. C* **2008**, *112*, 17281.
- [123] H. Sun, *J. Phys. Chem. B* **1998**, *102*, 7338.
- [124] P. Dauber-Osguthorpe, V. A. Roberts, D. J. Osguthorpe, J. Wolff, M. Genest, A. T. Hagler, *Proteins: Struct. Funct. Bioinf.* **1988**, *4*, 31.
- [125] K. Kubiak-Ossowska, P. A. Mulheran, W. Nowak, *J. Phys. Chem. B* **2014**, *118*, 9900.
- [126] a) A. Kyrychenko, *Phys. Chem. Chem. Phys.* **2015**, *17*, 12648; b) A. R. Mhashal, S. Roy, *PLoS One* **2014**, *9*, e114152.
- [127] a) J. Feng, J. M. Slocik, M. Sarikaya, R. R. Naik, B. L. Farmer, H. Heinz, *Small* **2012**, *8*, 1049; b) F. Ramezani, M. Amanlou, H. Rafii-Tabar, *J. Nanopart. Res.* **2014**, *16*, 2512.
- [128] J. Feng, R. B. Pandey, R. J. Berry, B. L. Farmer, R. R. Naik, H. Heinz, *Soft Matter* **2011**, *7*, 2113.
- [129] L. B. Wright, J. P. Palafox-Hernandez, P. M. Rodger, S. Corni, T. R. Walsh, *Chem. Sci.* **2015**.
- [130] H. Heinz, B. L. Farmer, R. B. Pandey, J. M. Slocik, S. S. Patnaik, R. Pachter, R. R. Naik, *J. Am. Chem. Soc.* **2009**, *131*, 9704.
- [131] M. J. Guberman-Pfeffer, J. Ulcickas, J. A. Gascón, *J. Phys. Chem. C* **2015**, *119*, 27804.
- [132] a) G. Nawrocki, M. Cieplak, *J. Phys. Chem. C* **2014**, *118*, 12929; b) O. D. Villarreal, L. Y. Chen, R. L. Whetten, M. J. Yacaman, *Phys. Chem. Chem. Phys.* **2015**, *17*, 3680; c) T. Popa, I. Paci, *J. Phys. Chem. C* **2015**, *119*, 9829; d) R. Gopalakrishnan, E. R. Azhagiya Singam, J. Vijaya Sundar, V. Subramanian, *Phys. Chem. Chem. Phys.* **2015**, *17*, 5172; e) T. Djebaili, J. Richardi, S. Abel, M. Marchi, *J. Phys. Chem. C* **2015**, *119*, 21146; f) T. Djebaili, J. Richardi, S. Abel, M. Marchi, *J. Phys. Chem. C* **2013**, *117*, 17791.
- [133] A. Vila Verde, J. M. Acres, J. K. Maranas, *Biomacromolecules* **2009**, *10*, 2118.
- [134] S. L. Mayo, B. D. Olafson, W. A. Goddard III, *J. Phys. Chem.* **1990**, *94*, 8897.
- [135] A. K. Rappé, C. J. Casewit, K. S. Colwell, W. A. Goddard III, W. M. Skiff, *J. Am. Chem. Soc.* **1992**, *114*, 10024.

- [136] P. M. Agrawal, B. M. Rice, D. L. Thompson, *Surf. Sci.* **2002**, *515*, 21.
- [137] J. Hautman, M. L. Klein, *J. Chem. Phys.* **1989**, *91*, 4994.
- [138] a) E. Benassi, G. Granucci, M. Persico, S. Corni, *J. Phys. Chem. C* **2015**, *119*, 5962; b) S. Pipolo, S. Corni, *Langmuir* **2014**, *30*, 4415.
- [139] M. V. Ivanov, M. R. Talipov, Q. K. Timerghazin, *J. Phys. Chem. A* **2015**, *119*, 1422.
- [140] a) O. Stueker, V. A. Ortega, G. G. Goss, M. Stepanova, *Small* **2014**, *10*, 2006; b) Z. Yang, Y. Li, G. Zhou, X. Chen, D. Tao, N. Hu, *J. Phys. Chem. C* **2015**, *119*, 1768.
- [141] a) M. Rosa, S. Corni, R. Di Felice, *J. Chem. Theory Comput.* **2014**, *10*, 1707; b) D. B. Kokh, S. Corni, P. J. Winn, M. Hoefling, K. E. Gottschalk, R. C. Wade, *J. Chem. Theory Comput.* **2010**, *6*, 1753.
- [142] Y. Shi, Z. Xia, J. Zhang, R. Best, C. Wu, J. W. Ponder, P. Ren, *J. Chem. Theory Comput.* **2013**, *9*, 4046.
- [143] G. A. Kaminski, R. A. Friesner, J. Tirado-Rives, W. L. Jorgensen, *J. Phys. Chem. B* **2001**, *105*, 6474.
- [144] a) S. Piana, K. Lindorff-Larsen, David E. Shaw, *Biophys. J.* **2011**, *100*, L47; b) A. D. Mackerell Jr., M. Feig, C. L. Brooks III, *J. Comput. Chem.* **2004**, *25*, 1400.
- [145] A. S. Barnard, X. M. Lin, L. A. Curtiss, *J. Phys. Chem. B* **2005**, *109*, 24465.
- [146] D. M. Kolb, *Prog. Surf. Sci.* **1996**, *51*, 109.
- [147] Y. Duan, C. Wu, S. Chowdhury, M. C. Lee, G. Xiong, W. Zhang, R. Yang, P. Cieplak, R. Luo, T. Lee, J. Caldwell, J. Wang, P. Kollman, *J. Comput. Chem.* **2003**, *24*, 1999.
- [148] X. Jiang, J. Gao, T. Huynh, P. Huai, C. Fan, R. Zhou, B. Song, *J. Chem. Phys.* **2014**, *140*, 234102.
- [149] S. K. Mudedla, E. R. Azhagiya Singam, K. Balamurugan, V. Subramanian, *Phys. Chem. Chem. Phys.* **2015**, *17*, 30307.
- [150] A. Perez, I. Marchan, D. Svozil, J. Sponer, T. E. Cheatham III, C. A. Laughton, M. Orozco, *Biophys. J.* **2007**, *92*, 3817.
- [151] a) S. Antonello, G. Arrigoni, T. Dainese, M. De Nardi, G. Parisio, L. Perotti, A. René, A. Venzo, F. Maran, *ACS Nano* **2014**, *8*, 2788; b) R. Ouyang, D.-e. Jiang, *J. Phys. Chem. C* **2015**, *119*, 21555; c) C. Liu, J. Lin, Y. Shi, G. Li, *Nanoscale* **2015**, *7*, 5987.
- [152] N. V. Perera, W. Isley, F. Maran, J. A. Gascón, *J. Phys. Chem. C* **2010**, *114*, 16043.
- [153] a) E. Heikkilä, A. A. Gurtovenko, H. Martinez-Seara, H. Häkkinen, I. Vattulainen, J. Akola, *J. Phys. Chem. C* **2012**, *116*, 9805; b) S. A. Alsharif, L. Y. Chen, A. Tlahuice-Flores, R. L. Whetten, M. J. Yacaman, *Phys. Chem. Chem. Phys.* **2014**, *16*, 3909.
- [154] A. C. T. van Duin, S. Dasgupta, F. Lorant, W. A. Goddard III, *J. Phys. Chem. A* **2001**, *105*, 9396.
- [155] T. T. Järvi, A. C. T. van Duin, K. Nordlund, W. A. Goddard III, *J. Phys. Chem. A* **2011**, *115*, 10315.
- [156] T. T. Järvi, A. Kuronen, M. O. Hakala, K. Nordlund, A. C. T. van Duin, W. A. Goddard III, T. Jacob, *Eur. Phys. J. B* **2008**, *66*, 75.
- [157] G.-T. Bae, C. M. Aikens, *J. Phys. Chem. A* **2013**, *117*, 10438.
- [158] S. Monti, V. Carravetta, H. Agren, *J. Phys. Chem. Lett.* **2016**, *272*.
- [159] Y. Han, D. Jiang, J. Zhang, W. Li, Z. Gan, J. Gu, *Front. Chem. Sci. Eng.* **2015**.
- [160] W. G. Noid, *J. Chem. Phys.* **2013**, *139*, 090901.
- [161] H. I. Ingólfsson, C. A. Lopez, J. J. Uusitalo, D. H. de Jong, S. M. Gopal, X. Periole, S. J. Marrink, *Wiley Interdiscip. Rev.: Comput. Mol. Sci.* **2014**, *4*, 225.
- [162] E. Brini, E. A. Algaer, P. Ganguly, C. Li, F. Rodríguez-Ropero, N. F. A. van der Vegt, *Soft Matter* **2013**, *9*, 2108.
- [163] S. J. Marrink, H. J. Risselada, S. Yefimov, D. P. Tieleman, A. H. de Vries, *J. Phys. Chem. B* **2007**, *111*, 7812.
- [164] a) S. J. Marrink, D. P. Tieleman, *Chem. Soc. Rev.* **2013**, *42*, 6801; b) J. J. Uusitalo, H. I. Ingólfsson, P. Akhshi, D. P. Tieleman, S. J. Marrink, *J. Chem. Theory Comput.* **2015**, *11*, 3932.
- [165] a) M. Enciso, A. Rey, *J. Chem. Phys.* **2012**, *136*, 215103; b) M. Enciso, A. Rey, *J. Chem. Phys.* **2013**, *139*, 115101.
- [166] a) T. A. Wassenaar, H. I. Ingólfsson, M. Prieß, S. J. Marrink, L. V. Schäfer, *J. Phys. Chem. B* **2013**, *117*, 3516; b) P. Sokkar, S. M. Choi, Y. M. Rhee, *J. Chem. Theory Comput.* **2013**, *9*, 3728; c) B. Ensing, S. O. Nielsen, P. B. Moore, M. L. Klein, M. Parrinello, *J. Chem. Theory Comput.* **2007**, *3*, 1100.
- [167] a) F. Tavanti, A. Pedone, M. C. Menziani, *New J. Chem.* **2015**, *39*, 2474; b) F. Tavanti, A. Pedone, M. C. Menziani, *J. Phys. Chem. C* **2015**, *119*, 22172.
- [168] R. C. Van Lehn, A. Alexander-Katz, *Soft Matter* **2011**, *7*, 11392.
- [169] a) J. Dong, J. Li, J. Zhou, *Langmuir* **2014**, *30*, 5599; b) H. Chan, P. Král, *Nanoscale* **2011**, *3*, 1881.
- [170] a) F. Simonelli, D. Bochicchio, R. Ferrando, G. Rossi, *J. Phys. Chem. Lett.* **2015**, *6*, 3175; b) J. Lin, A. Alexander-Katz, *ACS Nano* **2013**, *7*, 10799; c) E. L. da Rocha, G. F. Caramori, C. R. Rambo, *Phys. Chem. Chem. Phys.* **2013**, *15*, 2282; d) P. A. Oroskar, C. J. Jameson, S. Murad, *Langmuir* **2015**, *31*, 1074; e) J.-Q. Lin, Y.-G. Zheng, H.-W. Zhang, Z. Chen, *Langmuir* **2011**, *27*, 8323; f) J.-Q. Lin, H.-W. Zhang, Z. Chen, Y.-G. Zheng, Z.-Q. Zhang, H.-F. Ye, *J. Phys. Chem. C* **2011**, *115*, 18991.
- [171] a) R. C. Van Lehn, M. Ricci, P. H. J. Silva, P. Andreozzi, J. Reguera, K. Voitčhovsky, F. Stellacci, A. Alexander-Katz, *Nat. Commun.* **2014**, *5*, 4482; b) R. C. Van Lehn, A. Alexander-Katz, *J. Phys. Chem. B* **2014**, *118*, 12586.
- [172] J. M. D. Lane, G. S. Grest, *Nanoscale* **2014**, *6*, 5132.
- [173] a) B. Song, H. J. Yuan, S. V. Pham, C. J. Jameson, S. Murad, *Langmuir* **2012**, *28*, 16989; b) B. Song, H. Yuan, C. J. Jameson, S. Murad, *Mol. Phys.* **2012**, *110*, 2181.
- [174] Y. Li, X. Zhang, D. Cao, *Soft Matter* **2014**, *10*, 6844.
- [175] S. Kumar, D. Bouzida, R. H. Swendsen, P. A. Kollman, J. M. Rosenberg, *J. Comput. Chem.* **1992**, *13*, 1011.
- [176] a) A. Barducci, M. Bonomi, M. Parrinello, *Wiley Interdiscip. Rev.: Comput. Mol. Sci.* **2011**, *1*, 826; b) G. Bussi, F. L. Gervasio, A. Laio, M. Parrinello, *J. Am. Chem. Soc.* **2006**, *128*, 13435.
- [177] a) P. Liu, B. Kim, R. A. Friesner, B. J. Berne, *Proc. Natl. Acad. Sci. USA* **2005**, *102*, 13749; b) D. J. Earl, M. W. Deem, *Phys. Chem. Chem. Phys.* **2005**, *7*, 3910; c) X. Li, J. A. Snyder, S. J. Stuart, R. A. Latour, *J. Chem. Phys.* **2015**, *143*, 144105; d) A. H. Brown, T. R. Walsh, *Comput. Phys. Commun.* **2015**, *192*, 278; e) X. Li, R. A. Latour, S. J. Stuart, *J. Chem. Phys.* **2009**, *130*, 174106; f) X. Li, C. P. O'Brien, G. Collier, N. A. Vellore, F. Wang, R. A. Latour, D. A. Bruce, S. J. Stuart, *J. Chem. Phys.* **2007**, *127*, 164116.
- [178] M. J. Penna, M. Mijajlovic, M. J. Biggs, *J. Am. Chem. Soc.* **2014**, *136*, 5323.
- [179] a) R. C. Bernardi, M. C. R. Melo, K. Schulten, *Biochim. Biophys. Acta Gen. Subj.* **2014**, *1850*, 872; b) V. Spiwok, Z. Sucur, P. Hosek, *Biotechnol. Adv.* **2015**, *33*, 1130; c) M. Luitz, R. Bomblies, K. Ostermeir, M. Zacharias, *J. Phys.: Condens. Matter* **2015**, *27*, 323101.
- [180] a) L. B. Wright, N. A. Merrill, M. R. Knecht, T. R. Walsh, *ACS Appl. Mater. Interfaces* **2014**, *6*, 10524; b) G. Brancolini, L. Z. Polzi, S. Corni, J. Self-Assem. Mol. Electron. **2015**, *2*, 1; c) M. Hoefling, F. Iori, S. Corni, K.-E. Gottschalk, *Langmuir* **2010**, *26*, 8347.
- [181] a) R. B. Pandey, H. Heinz, J. Feng, B. L. Farmer, J. M. Slocik, L. F. Drummy, R. R. Naik, *Phys. Chem. Chem. Phys.* **2009**, *11*, 1989; b) A. Vila Verde, P. J. Beltramo, J. K. Maranas, *Langmuir* **2011**, *27*, 5918; c) R. Braun, M. Sarikaya, K. Schulten, *J. Biomater. Sci. Polym. Ed.* **2002**, *13*, 747.
- [182] a) V. P. Raut, M. A. Agashe, S. J. Stuart, R. A. Latour, *Langmuir* **2005**, *21*, 1629; b) S. Corni, M. Hnilova, C. Tamerler, M. Sarikaya, *J. Phys. Chem. C* **2013**, *117*, 16990.
- [183] H. Andresen, M. Mager, M. Grießner, P. Charchar, N. Todorova, N. Bell, G. Theocharidis, S. Bertazzo, I. Yarovsky, M. M. Stevens, *Chem. Mater.* **2014**, *26*, 4696.
- [184] L. B. Wright, P. M. Rodger, T. R. Walsh, *RSC Adv.* **2013**, *3*, 16399.
- [185] J.-W. Park, J. S. Shumaker-Parry, *J. Am. Chem. Soc.* **2014**, *136*, 1907.

- [186] L. B. Wright, P. M. Rodger, T. R. Walsh, *Langmuir* **2014**, *30*, 15171.
- [187] G. Brancolini, A. Corazza, M. Vuano, F. Fogolari, M. C. Mimmi, V. Bellotti, M. Stoppini, S. Corni, G. Esposito, *ACS Nano* **2015**, *9*, 2600.
- [188] S.-T. Wang, Y. Lin, N. Todorova, M. Mazo, Y. Xu, V. Leonardo, N. Amdursky, I. Yarovsky, M. M. Stevens, in preparation.
- [189] W. Lin, T. Insley, M. D. Tuttle, L. Zhu, D. A. Berthold, P. Král, C. M. Rienstra, C. J. Murphy, *J. Phys. Chem. C* **2015**, *119*, 21035.
- [190] a) M. E. Siwko, S. Corni, *Phys. Chem. Chem. Phys.* **2013**, *15*, 5945; b) L. Zanetti-Polzi, I. Daidone, C. A. Bortolotti, S. Corni, *J. Am. Chem. Soc.* **2014**, *136*, 12929; c) C. Peng, J. Liu, J. Zhou, *J. Phys. Chem. C* **2015**, *119*, 20773.
- [191] A. Hung, S. Mwenifumbo, M. Mager, J. J. Kuna, F. Stellacci, I. Yarovsky, M. M. Stevens, *J. Am. Chem. Soc.* **2011**, *133*, 1438.
- [192] A. Hung, M. Mager, M. Hembury, F. Stellacci, M. M. Stevens, I. Yarovsky, *Chem. Sci.* **2013**, *4*, 928.
- [193] J. J. Kuna, K. Voitchovsky, C. Singh, H. Jiang, S. Mwenifumbo, P. K. Ghorai, M. M. Stevens, S. C. Glotzer, F. Stellacci, *Nat. Mater.* **2009**, *8*, 837.
- [194] N. Todorova, C. Chiappini, M. Mager, B. Simona, I. I. Patel, M. M. Stevens, I. Yarovsky, *Nano Lett.* **2014**, *14*, 5229.
- [195] a) N. A. Brooks, D. S. Pouniotis, C.-K. Tang, V. Apostolopoulos, G. A. Pietersz, *Biochim. Biophys. Acta Rev. Cancer* **2010**, *1805*, 25; b) Ž. Krpetić, S. Saleemi, I. A. Prior, V. Séé, R. Qureshi, M. Brust, *ACS Nano* **2011**, *5*, 5195; c) J. M. de la Fuente, C. C. Berry, *Bioconjugate Chem.* **2005**, *16*, 1176.
- [196] R. C. Van Lehn, P. U. Atukorale, R. P. Carney, Y.-S. Yang, F. Stellacci, D. J. Irvine, A. Alexander-Katz, *Nano Lett.* **2013**, *13*, 4060.
- [197] a) R. C. Van Lehn, A. Alexander-Katz, *J. Phys. Chem. C* **2013**, *117*, 20104; b) R. C. Van Lehn, A. Alexander-Katz, *J. Phys. Chem. A* **2014**, *118*, 5848; c) R. C. Van Lehn, A. Alexander-Katz, *Soft Matter* **2014**, *10*, 648; d) R. C. Van Lehn, A. Alexander-Katz, *Soft Matter* **2015**, *11*, 3165.
- [198] A. Heuer-Jungemann, P. K. Harimech, T. Brown, A. G. Kanaras, *Nanoscale* **2013**, *5*, 9503.
- [199] R. Elghanian, J. J. Storhoff, R. C. Mucic, R. L. Letsinger, C. A. Mirkin, *Science* **1997**, *277*, 1078.
- [200] O. S. Lee, T. R. Prytkova, G. C. Schatz, *J. Phys. Chem. Lett.* **2010**, *1*, 1781.
- [201] a) O. S. Lee, V. Y. Cho, G. C. Schatz, *J. Phys. Chem. B* **2012**, *116*, 7000; b) V. A. Ngo, R. K. Kalia, A. Nakano, P. Vashishta, *J. Phys. Chem. C* **2012**, *116*, 19579.
- [202] A. J. Makarucha, N. Todorova, I. Yarovsky, *Eur. Biophys. J.* **2011**, *40*, 103.
- [203] S. Linse, C. Cabaleiro-Lago, W.-F. Xue, I. Lynch, S. Lindman, E. Thulin, S. E. Radford, K. A. Dawson, *Proc. Natl. Acad. Sci. USA* **2007**, *104*, 8691.
- [204] T. P. J. Knowles, M. Vendruscolo, C. M. Dobson, *Nat. Rev. Mol. Cell Biol.* **2014**, *15*, 384.
- [205] R. Vácha, S. Linse, M. Lund, *J. Am. Chem. Soc.* **2014**, *136*, 11776.
- [206] a) E. Boisselier, D. Astruc, *Chem. Soc. Rev.* **2009**, *38*, 1759; b) Y. Xia, W. Li, C. M. Cobley, J. Chen, X. Xia, Q. Zhang, M. Yang, E. C. Cho, P. K. Brown, *Acc. Chem. Res.* **2011**, *44*, 914; c) C. Zhang, C. Li, Y. Liu, J. Zhang, C. Bao, S. Liang, Q. Wang, Y. Yang, H. Fu, K. Wang, D. Cui, *Adv. Funct. Mater.* **2015**, *25*, 1314.
- [207] M. Hoefling, S. Monti, S. Corni, K. E. Gottschalk, *PLoS One* **2011**, *6*, e20925.
- [208] S. Mirsadeghi, R. Dinarvand, M. H. Ghahremani, M. R. Hormozi-Nezhad, Z. Mahmoudi, M. J. Hajipour, F. Atyabi, M. Ghavami, M. Mahmoudi, *Nanoscale* **2015**, *7*, 5004.
- [209] H. Y. Mao, S. Laurent, W. Chen, O. Akhavan, M. Imani, A. A. Ashkarran, M. Mahmoudi, *Chem. Rev.* **2013**, *113*, 3407.
- [210] M. Mahmoudi, M. P. Monopoli, M. Rezaei, I. Lynch, F. Bertoli, J. J. McManus, K. A. Dawson, *ChemBioChem* **2013**, *14*, 568.
- [211] F. Ramezani, H. Rafii-Tabar, *Mol. BioSyst.* **2015**, *11*, 454.
- [212] O. Carrillo-Parramon, G. Brancolini, S. Corni, *BioNanoSci.* **2013**, *3*, 12.
- [213] J. R. Perilla, B. C. Goh, C. K. Cassidy, B. Liu, R. C. Bernardi, T. Rudack, H. Yu, Z. Wu, K. Schulten, *Curr. Opin. Struct. Biol.* **2015**, *31*, 64.
- [214] E. H. Lee, J. Hsin, M. Sotomayor, G. Comellas, K. Schulten, *Structure* **2009**, *17*, 1295.
- [215] M. Praprotnik, L. Delle Site, K. Kremer, *J. Chem. Phys.* **2005**, *123*, 224106.

Received: November 25, 2015

Revised: February 1, 2016

Published online: